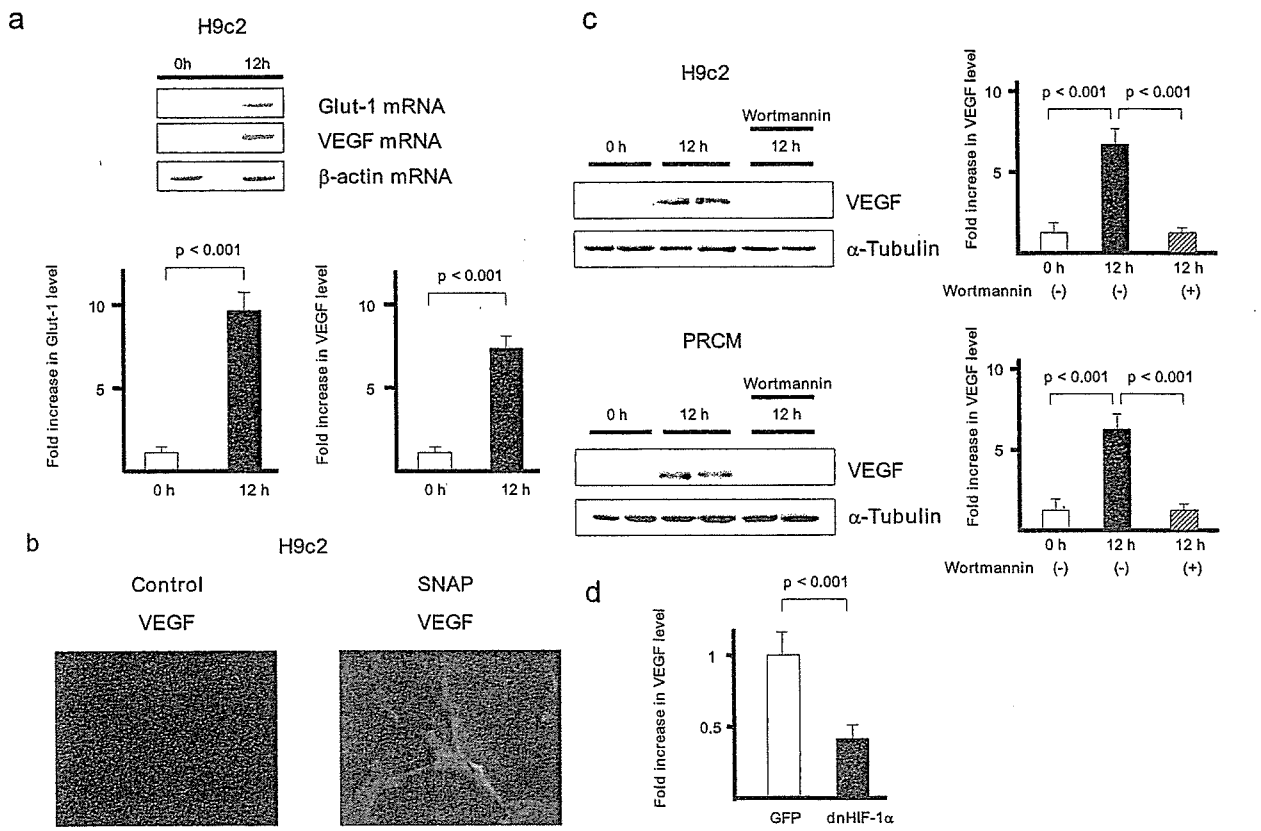

Fig. 4. SNAP increases Glut-1 and VEGF gene expression levels through HIF-1α in cardiomyocytes under normoxia. In H9c2 cells, Glut-1 mRNA and VEGF mRNA were both increased by SNAP ($n = 5$) (**a**). VEGF immunoreactivity was increased by SNAP in H9c2 cells ($n = 5$) (**b**). The SNAP-induced VEGF protein expression, which was also observed in PRCMs, was completely inhibited by 30 nM wortmannin ($n = 5$) (**c**). In contrast to control (GFP), VEGF induction by SNAP was blocked by dn HIF-1α in HEK293 cells ($n = 5$) (**d**).

(SNAP group) revealed increased Flk-1 phosphorylation (a fourfold increase compared to the control group, $p < 0.001$, $n = 5$), a VEGF type-2 receptor responsible for angiogenesis, in HUVECs (Fig. 5a). Furthermore, HUVECs were cultured on Matrigel in the presence of conditioned medium. Compared with the control group, the SNAP group activated more angiogenesis. It is suggested that SNAP exerts an acceleration of angiogenesis partially via cardiomyocyte-derived angiogenic factors, including VEGF (Fig. 5b).

DISCUSSION

It is well known that NO plays a critical role in modulating the vascular tone. According to the vascular effect, the depressed functional capacity of NO production would result in vasoconstriction and poor collateral circulation. Therefore NO or a NO donor has been used for coronary vasodilatation and decreasing blood pressure in systemic or pulmonary hypertension. However, the other effect of NO or a NO donor on cardiomyocytes remains to be fully investigated. It is known that NO is synthesized through eNOS in endothelial cells, and it is speculated that it has a significant paracrine effect on cardiomyocytes; however, it is unclear whether cardiomyocyte-derived NO possesses the direct action on cardiomyocytes to produce angiogenic factors.

Our previous study demonstrated the involvement of PI3K-Akt pathway in inducing the expression of HIF-1α by ACh during normoxia [4]. In the present study, SNAP-treated cardiomyocytes revealed a similar pathway in the induction of HIF-1α, suggesting that NO from cardiomyocytes activates an angiogenic signaling through HIF-1α.

As shown in the present study using DAF-2, a NO-sensitive dye, NO was detected in cardiomyocytes in response to SNAP as well as ACh, suggesting that cardiomyocytes release NO. The NO release by SNAP appeared in a rapid time course 30 min after the treatment, and it was not detected in PRCMs pretreated with L-NAME. Other studies have also reported the inhibitory effects of L-NAME on SNAP without the exact mechanisms being identified [24–27]; however, the speculated mechanism could be that the L-NAME pretreatment for 60 min of PRCMs might inhibit NO synthase, thereby reducing the basal NO production. Even if SNAP was thereafter added for 30 min to enhance NO release, the NO level in

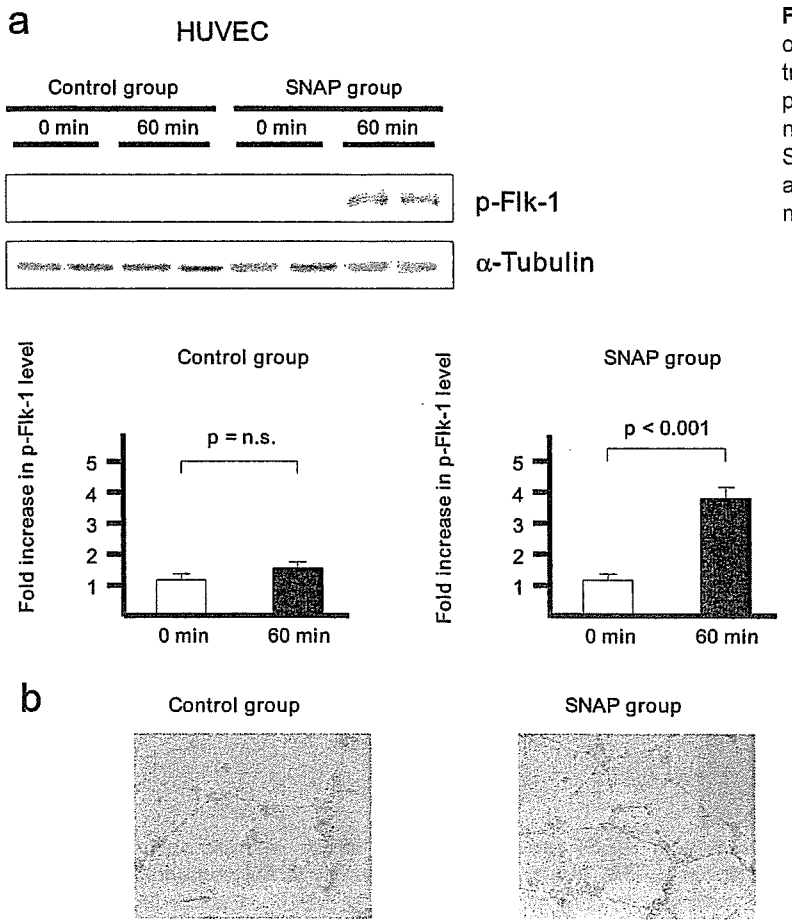

Fig. 5. VEGF derived from SNAP-treated cardiomyocytes induces angiogenesis. The SNAP-treated conditioned medium increased Flk-1 phosphorylation in HUVECs, compared with the nontreated conditioned medium (n = 5) (**a**). The SNAP-treated conditioned medium accelerated angiogenesis in HUVECs compared with the nontreated conditioned medium (**b**).

the treated cardiomyocyte might be too low, compared with the nontreated cell, to be detected by DAF-2. Therefore, these results suggest that cardiomyocyte-derived NO as a paracrine or autocrine effector plays a critical role in the HIF-1α induction in cardiomyocytes.

Second, as shown in this study, NO increased the cardiac VEGF protein expression through HIF-1α regulation, and dn HIF-1α decreased the VEGF expression by SNAP. VEGF itself has been reported to be involved in cell survival through the tyrosine kinase receptors, including VEGF type-2 receptor (Flk-1), activating Akt via a PI3K-dependent pathway [28], leading to eNOS upregulation. Furthermore, as suggested in our study, the cardiomyocyte-derived VEGF plays a crucial role in accelerating angiogenesis by endothelial cells in a paracrine fashion because VEGF produced by cardiomyocytes phosphorylated Flk-1 in HUVECs. These results suggest that cardiomyocytes can not only be a target for a NO donor to activate a nonhypoxic pathway of HIF-1α, but can also play a role in producing angiogenic factors in the heart. Taken together, the beneficial effects of NO might in part be a result of the cell signaling through PI3K-Akt, and also in part a result of the angiogenic signaling through HIF-1α–VEGF.

In the recent study by Giordano *et al.* [29], a cardiomyocyte-specific knockout of VEGF caused impaired cardiac development with hypovascularity in the heart, suggesting that cardiomyocyte-induced VEGF production is essential for cardiac development; however, their study did not reveal the precise cellular mechanism by which cardiac VEGF deletion leads to hypovasculature and depressed cardiac function. Our present study indicated that HIF-1α induction through NO plays a main role in stimulating VEGF production by cardiomyocytes and accelerates angiogenesis.

In this study we focused on HIF-1α as an upstream factor regulating cardiac VEGF expression. Unlike the hypoxic induction pathway of HIF-1α, there is no direct evidence for a nonhypoxic induction pathway of cardiomyocytes through NO involved in angiogenesis. Consequently, this study revealed another pathway of cardiac HIF-1α induction. PI3K-Akt signal has many aspects in cell survival, including an antiapoptotic activity, such as an inhibition of Bad-binding to Bcl-2 through Akt phosphorylation, an inhibition of proapoptotic caspases, including caspase 9 and Fas, and an inhibition of the activity of proapoptotic glycogen synthetase kinase-3 [30, 31]. In previous studies, which used other cell lines, the PI3K-

Akt pathway has been demonstrated to be involved in the NO-dependent stabilization of HIF-1α [14, 32–34]. As demonstrated in this study, in the presence of actinomycin D, the dose of which is adequate to inhibit transcriptional activity, SNAP posttranslationally regulated HIF-1α. Actinomycin D was used to identify which mechanisms are responsible for the increased protein expression, i.e., de novo synthesis or posttranslational modification. The protein level of HIF-1α was not decreased by actinomycin D; therefore this suggests that SNAP does not play a role in the transcriptional regulation of HIF-1α, rather in the inhibition of protein degradation. Therefore in cardiomyocytes, such a mechanism might be involved in a NO-mediated Akt-HIF-1α-VEGF signaling pathway, leading to cell protection.

In conclusion, it is suggested that NO has beneficial effects on cardiomyocytes by the activation of the nonhypoxic HIF-1α induction pathway, and furthermore, it contributes to angiogenesis through cardiac VEGF production, which phosphorylates Flk-1, a VEGF type-2 receptor.

This study was supported by a Health and Labor Sciences Research Grant (H15-PHYSI-001) for Advanced Medical Technology from the Ministry of Health, Labor, and Welfare of Japan.

REFERENCES

1. Julian DG, Gamm AJ, Frangin G, Janse MJ, Munoz A, Schwartz PJ, Simon P. Randomised trial of effect of amiodarone on mortality in patients with left-ventricular dysfunction after recent myocardial infarction: EMIAT. European Myocardial Infarct Amiodarone Trial Investigators. Lancet. 1997;349:667-74.
2. Li M, Zheng C, Sato T, Kawada T, Sugimachi M, Sunagawa K. Vagal nerve stimulation markedly improves long-term survival after chronic heart failure in rats. Circulation. 2004;109:120-4.
3. Krieg T, Qin Q, Philipp S, Alexeyev MF, Cohen MV, Downey JM. Acetylcholine and bradykinin trigger preconditioning in the heart through a pathway that includes Akt and NOS. Am J Physiol Heart Circ Physiol. 2004;287:H2606-11.
4. Kakinuma Y, Ando M, Kuwabara M, Rajesh G, Okudela K, Kobayashi M, Sato T. Acetylcholine from vagal stimulation protects cardiomyocytes against ischemic and hypoxia involving additive non-hypoxic condition of HIF-1α. FEBS Lett. 2005;579:2111-8.
5. Semenza GL. Hypoxia-inducible factor 1. oxygen homeostasis and disease pathophysiology. Trends Mol Med. 2001;7:345-50.
6. Ferrara N, Houck K, Jakeman L, Leung DW. Molecular and biological properties of the vascular endothelial growth factor family of proteins. Endocr Rev. 1992;13:18-32.
7. Wang GL, Jiang BH, Rue EA, Semenza GL. Hypoxia-inducible factor 1 is a basic-helix-loop-helix-PAS heterodimer regulated by cellular O_2 tension. Proc Natl Acad Sci USA. 1995;92:5510-4.
8. Maxwell PH, Wiesener MS, Chang GW, Clifford SC, Vaux EC, Cockman ME, Wykoff CC, Pugh CW, Maher ER, Ratcliffe PJ. The tumour suppressor protein VHL targets hypoxia-inducible factors for oxygen-dependent proteolysis. Nature. 1999;399:271-5.
9. Ivan M, Kondo K, Yang H, Kim W, Valiando J, Ohh M, Salic A, Asara JM, Lane WS, Kaelin Jr WG. HIF-1α targeted for VHL-mediated destruction by proline hydroxylation: Implications for O_2 sensing. Science. 2001;292:464-8.
10. Cantley LC, Auger KR, Carpenter C, Duckworth B, Graziani A, Kapeller R, Soltoff S. Oncogenes and signal transduction. Cell. 1991;64:281-302.
11. Yao R, Cooper GM. Requierment for phosphatidylinositol-3 kinase in the prevention of apoptosis by nerve growth factor. Science. 1995;267:2003-6.
12. Kandel ES, Hay N. The regulation and activities of the multifunctional serine/threonine kinase Akt/PKB. Exp Cell Res. 1999;253:210-29.
13. Richard DE, Berra E, Pouysségur J. Nonhypoxic pathway mediates the induction of hypoxia-inducible factor 1α in vascular smooth muscle cells. J Biol Chem. 2000;275:26765-71.
14. Sandau KB, Zhou J, Kietzmann T, Brune B. Regulation of the hypoxia-inducible factor 1 alpha by the inflammatory mediators nitric oxide and tumor necrosis factor-alpha in contrast to desferroxamine and phenylarsine oxide. J Biol Chem. 2001;276:39805-11.
15. Sandau KB, Fandrey J, Brune B. Accumulation of HIF-1alpha under the influence of nitric oxide. Blood. 2001;97:1009-15.
16. Balligand JL, Cannon PJ. Nitric oxide synthases and cardiac muscle: Autocrine and paracrine influences. Arterioscler Thromb Vasc Biol. 1997;17:1846-58.
17. Kakinuma Y, Miyauchi T, Yuki K, Murakoshi M, Goto K, Yamaguchi I. Novel molecular mechanism of increased myocardial endothelin-1 expression in the failing heart involving the transcriptional factor HIF-1α induced for impaired myocardial energy metabolism. Circulation. 2001; 103:2387-4.
18. Ilangovan G, Osinbowale S, Bratasz A, Bonar M, Cardounel AJ, Zweier JL, Kuppusamy P. Heat shock regulates the respiration of cardiac H9c2 cells through upregulation of nitric oxide synthase. Am J Physiol Cell Physiol. 2004;287:C1472-81.
19. Wu G, Mannam AP, Wu J, Kirbis S, Shie JL, Chen C, Laham RJ, Sellke FW, Li J. Hypoxia induces myocyte-dependent COX-2 regulation in endothelial cells: role of VEGF. Am J Physiol Heart Circ Physiol. 2003;285:H2420-H9.
20. Kimura C, Koyama T, Oike M, Ito Y. Hypotonic stress-induced NO production in endothelium depends on endogenous ATP. Biochem Biophys Res Commun. 2000;274:736-40.
21. Chachami G, Simos G, Hatziefthimiou A, Bonanou S, Molyvdas PA, Paraskeva E. Cobalt induces hypoxia-inducible factor-1alpha expression in airway smooth muscle cells by a reactive oxygen species and PI3K-dependent mechanism. Am J Respir Cell Mol Biol. 2004;31:544-51.
22. Weller R, Schwentker A, Billiar TR, Vodovotz Y. Autologous nitric oxide protects mouse and human keratinocytes from ultraviolet B radiation-induced apoptosis. Am J Physiol Cell Physiol. 2003;284:C1140-8.
23. Chen J, Zhao S, Nakada K, Kuge Y, Tamaki N, Okada F, Wang J, Shindo M, Higashino F, Takeda K, Asaka M, Katoh H, Sugiyama T, Hosokawa M, Kobayashi M. Dominant-negative hypoxia-inducible factor-1 alpha reduces tumorigenicity of pancreatic cancer cells through the suppression of glucose metabolism. Am J Pathol. 2004;162:1283-91.
24. Dang VC *et al.* Nitric oxide-cGMP-protein kinase G signaling pathway induces anoxic preconditioning through activation of ATP-sensitive K^+ channels in rat hearts. Am J Physiol Heart Circ Physiol. (Epub) Dec 9. 2005.
25. Chen J, Zhu JX, Wilson I, Cameron JS. Cardioprotective effects of K_{ATP} channel activation during hypoxia in goldfish carassius auratus. J Exp Biol. 2005;208:2765-72.
26. Maejima Y *et al.* Nitric oxide inhibits ischemia/reperfusion-induced myocardial apoptosis by modulating cyclin A-associated kinase activity. Cardiovasc Res. 2003;59:308-20.
27. Ebihara Y *et al.* Modulation of endothelin-a effects on rat hearts and cardiomyocytes by nitric oxide and 8-bromo cyclic GMP. J Mol Cell Cardiol. 1996;28:265-77.
29. Gerber HP, McMurtrey A, Kowalski J, Yan M, Kety BA, Dixit V, Ferrara N. Vascular endothelial growth factor regulates endothelial cell survival through the phosphatidyl-inositol 3'-kinase/Akt signal transduction pathway. Requirement for Flk-1/KDR activation. J Biol Chem. 1998;273:30336-43.
29. Giordano FJ, Gerber HP, Williams SP, VanBruggen N, Bunting S, Ruiz-Lozano P, Gu Y, Nath AK, Huang Y, Hickey R, Dalton N, Peterson KL, Ross J Jr, Chien KR, Ferrara N. A cardiac myocyte vascular endothelial growth factor paracrine pathway is required to maintain cardiac function. Proc Natl Acad Sci USA. 2001;98:5780-5.
30. Kennedy SG, Wagner AJ, Conzen SD, Jordan J, Bellacosa A, Tsichlis PN, Hay N. The PI3-kinase/Akt signaling pathway delivers an anti-apoptotic signal. Genes Dev. 1997;11:701-13.
31. Cross DA, Alessi DR, Cohen P, Andjelkovich M, Hemmings BA. Inhibition of glycogen synthase kinase-3 by insulin mediated by protein kinase B. Nature. 1995;378:785-9.
32. Kasuno K, Takabuchi S, Fukuda K, Kizaka-Kondoh S, Yodoi J, Adachi T, Semenza GL, Hirota K. Nitric oxide induces hypoxia-inducible factor 1 activation that is dependent on MAPK and phosphatidylinositol 3-kinase signaling. J Biol Chem. 2004;279:2550-8.
33. Sandau KB, Faus HG, Brune B. Induction of hypoxia-inducible-factor 1 by nitric oxide is mediated via the PI3K pathway. Biochem Biophys Res Commun. 2000;278:263-7.
34. Matzen E, Zhou J, Jelkmann W, Fandrey J, Brune B. Nitric oxide impairs normoxic degradation of HIF-1α by inhibition of prolyl hydroxylases. Mol Biol Cell. 2003;14:3470-81.

Artificial Baroreflex

Clinical Application of a Bionic Baroreflex System

Fumiyasu Yamasaki, MD; Takahiro Ushida, MD; Takeshi Yokoyama, DDS; Motonori Ando, PhD; Koichi Yamashita, MD; Takayuki Sato, MD

Background—We proposed a novel therapeutic strategy against central baroreflex failure: implementation of an artificial baroreflex system to automatically regulate sympathetic vasomotor tone, ie, a bionic baroreflex system (BBS), and we tested its efficacy in a model of sudden hypotension during surgery.

Methods and Results—The BBS consisted of a computer-controlled negative-feedback circuit that sensed arterial pressure (AP) and automatically computed the frequency (STM) of a pulse train required to stimulate sympathetic nerves via an epidural catheter placed at the level of the lower thoracic spinal cord. An operation rule was subsequently designed for the BBS using a feedback correction with proportional and integral gain factors. The transfer function from STM to AP was identified by a white noise system identification method in 12 sevoflurane-anesthetized patients undergoing orthopedic surgery involving the cervical vertebrae, and the feedback correction factors were determined with a numerical simulation to enable the BBS to quickly and stably attenuate an external disturbance on AP. The performance of the designed BBS was then examined in a model of orthostatic hypotension during knee joint surgery (n=21). Without the implementation of the BBS, a sudden deflation of a thigh tourniquet resulted in a 17±3 mm Hg decrease in AP within 10 seconds and a 25±2 mm Hg decrease in AP within 50 seconds. By contrast, during real-time execution of the BBS, the decrease in AP was 9±2 mm Hg at 10 seconds and 1±2 mm Hg at 50 seconds after the deflation.

Conclusions—These results suggest the feasibility of a BBS approach for central baroreflex failure. (***Circulation.*** **2006; 113:634-639.)**

Key Words: baroreceptors ■ blood pressure ■ computers ■ electrical stimulation ■ nervous system, sympathetic

The arterial baroreflex acts to maintain cerebral perfusion by quickly attenuating the effect of an external disturbance, such as the assumption of an upright position, on arterial pressure (AP).[1–4] Therefore, functional restoration of dynamic properties of the arterial baroreflex is essential for the treatment of patients with various syndromes of baroreflex failure,[5] including Shy-Drager syndrome,[6–9] baroreceptor deafferentation,[10,11] and traumatic spinal cord injuries.[12,13] However, most commonly used interventions, including salt loading,[14,15] cardiac pacing,[16,17] and adrenergic agonists,[18,19] can neither restore nor reproduce the functioning of the native vasomotor center, and most affected patients remain bedridden.

Clinical Perspective p 639

We recently developed a framework for identifying an operational rule of the vasomotor center and a prototype of a bionic baroreflex system (BBS) in rats.[20–22] The BBS consisted of a negative-feedback system controlled by a computer (ie, the artificial vasomotor center) that sensed AP and automatically computed the frequency of a pulse train required to stimulate sympathetic efferent nerves through a pair of wire electrodes placed in the celiac ganglion. Previous experimental work demonstrated that the BBS restored native baroreflex function in rats with central baroreflex failure; however, an applicable neural interface with quick and effective controllability of AP is required for application of this technology in the clinical setting. The goal of the present study was to determine the efficacy of a novel bionic technology for the intraoperative restoration of AP in the context of central baroreflex failure and to validate this technology in a clinical model of orthostatic hypotension.

Methods

All studies were approved by the institutional review committee, and all subjects gave informed consent.

Theoretical Considerations

As previously described,[20–22] the principle of the BBS is based on a negative-feedback mechanism (Figure 1). The instantaneous AP is measured by a pressure transducer connected to a computer that functions as a controller or artificial vasomotor center. Instead of the disabled native vasomotor center, the controller automatically exe-

Received September 8, 2005; revision received October 31, 2005; accepted November 21, 2005.

From the Departments of Cardiovascular Control (F.Y., M.A., T.S.), Clinical Laboratory (F.Y.), Orthopedic Surgery (T.U.), and Anesthesiology (T.Y., K.Y.), Kochi Medical School, Nankoku, Japan.

Correspondence to Fumiyasu Yamasaki, MD, Department of Clinical Laboratory, Kochi Medical School, Nankoku 783-8505, Japan. E-mail yamasakf@med.kochi-u.ac.jp

Circulation **is available at http://www.circulationaha.org** **DOI: 10.1161/CIRCULATIONAHA.105.587915**

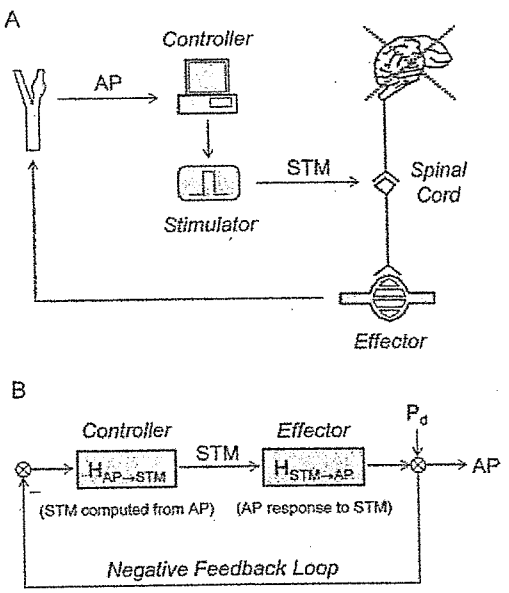

Figure 1. Schematic illustration (A) and block diagram (B) of a BBS. In the context of central baroreflex failure, the BBS automatically computes the frequency (STM) of a pulse train to stimulate sympathetic nerves through an epidural catheter placed at the level of lower thoracic spinal cord, while simultaneously sensing the change in AP. $H_{AP\rightarrow STM}$ denotes a transfer function for the controller functioning as an artificial vasomotor center. $H_{STM\rightarrow AP}$ is a transfer function showing the dynamic response of AP to STM. The overall transfer function of the BBS is given by $H_{AP\rightarrow STM}\times H_{STM\rightarrow AP}$. Therefore, the effect of an external disturbance (P_d) on AP is attenuated to $1/(1+H_{AP\rightarrow STM}\times H_{STM\rightarrow AP})$.

cutes real-time operations that determine the frequency of electrical stimulation (STM) required to minimize the effect of an external disturbance (P_d) on AP and then commands an electrical stimulator to deliver a stimulus of the same frequency to the vasomotor sympathetic nerves via epidural-catheter electrodes placed at the lower thoracic level of the spinal cord. The lower thoracic level was selected as the site for the neural interface of the BBS because the abdominal splanchnic vascular bed is a major effector mechanism for the arterial baroreflex.[23–25]

According to a classic feedback-control theory, ie, feedback correction with proportional and integral gain factors,[26,27] the following algorithm was used to program the controller for the calculation of STM in the frequency domain:

$$(1)\qquad H_{AP\rightarrow STM}=K_p+\frac{K_i}{2\pi fj}$$

where $H_{AP\rightarrow STM}$ is a transfer function from AP to STM, K_p is the proportional correction factor, K_i is the integral correction factor, and j is the imaginary unit. The proportional factor determines the feedback amplification based on the absolute value of the instantaneous control error due to P_d, and the integral factor adjusts the feedback amplification based on the cumulative value of the instantaneous control error. Therefore, STM is computed as follows:

$$(2)\qquad STM=-AP\cdot H_{AP\rightarrow STM}$$

and AP is also expressed as follows:

$$(3)\qquad AP=STM\cdot H_{STM\rightarrow AP}+P_d$$

where $H_{STM\rightarrow AP}$ denotes the frequency response of AP to STM. From Equations 2 and 3, the effect of P_d on AP is estimated as follows:

$$(4)\qquad AP=\frac{1}{1+H_{AP\rightarrow STM}\cdot H_{STM\rightarrow AP}}P_d$$

Thus, if $H_{AP\rightarrow STM}\cdot H_{STM\rightarrow AP}$ is far larger than unity, the BBS can nullify the effect of P_d on AP.

Subjects and Experimental Protocols

A total of 33 patients (46 to 84 years old, 19 males) who underwent orthopedic operations were enrolled in the present study. Ten patients had hypertension, and 4 had diabetes mellitus. None of the subjects had frequent ectopic beats or atrial fibrillation. After induction anesthesia with propofol, an endotracheal tube was introduced orally. The patients were mechanically ventilated with 67% nitrous oxide and 1.5% to 2% end-tidal sevoflurane in oxygen during experimental protocols, while end-tidal carbon dioxide was maintained at 35 to 38 mm Hg. An arterial catheter was placed in the radial artery for AP measurement. To record central venous pressure (CVP), a central venous catheter was placed in the femoral vein, and the tip of the catheter was advanced into the inferior vena cava just above the diaphragmatic level. Furthermore, an epidural catheter was placed percutaneously, and the tip, which contained a pair of electrodes (Unique Medical, Tokyo; interelectrode distance 15 mm), was placed at the level of Th_{9-11}. Placement of the central venous catheter and the epidural catheter was verified by chest radiograph.[28]

Before making an incision of affected areas, we performed 2 different protocols in separate groups of patients. In the first group of patients (n=12, 46 to 76 years old, 7 males) undergoing operations for cervical spondylosis and canal stenosis, the averaged $H_{STM\rightarrow AP}$ was estimated and the $H_{AP\rightarrow STM}$ was designed parametrically with Equation 1 to minimize the effect of P_d on AP. After we programmed the designed $H_{AP\rightarrow STM}$ into the computer, the efficacy of the BBS was tested against the rapid progressive hypotension induced by use of a thigh tourniquet[29–31] in the second group of patients (n=21, 64 to 84 years old, 12 males) undergoing operation for knee joint osteoarthritis. During each protocol, the muscle twitches induced by spinal cord stimulation were prevented by the intravenous administration of vecuronium bromide. Analgesia for the pain provoked by spinal cord stimulation and tourniquet inflation was provided by intravenous injection of fentanyl citrate. In a preliminary study, the validity of the analgesic preparation was confirmed for the experimental protocols, and the safety of spinal cord stimulation for 20 minutes was verified.

Estimation of Transfer Function From STM to AP

To characterize the dynamic nature of the AP response to STM, ie, $H_{STM\rightarrow AP}$, the lower thoracic sympathetic nerves were randomly stimulated for 15 minutes while we recorded AP. According to a white noise method for system identification, the STM was altered between 0 and 20 Hz every 4 seconds. The pulse width of electrical stimuli was fixed at 0.1 ms. The stimulation current was adjusted for each patient so as to produce a pressor response of ≈10 mm Hg at 20 Hz. This resulted in an average current of 15±4 (mean±SD) mA. The electrical signals of STM and AP were digitized at 100 Hz. As described previously,[20–22] the transfer function from STM to AP, $H_{STM\rightarrow AP}$, was estimated with a fast Fourier transform algorithm. Finally, the average of $H_{STM\rightarrow AP}$ among 12 patients was calculated.

Design of Artificial Vasomotor Center

With substitution of the averaged $H_{STM\rightarrow AP}$ for Equation 4, the instantaneous AP response to P_d was simulated numerically, and a stepwise decline with an amplitude of 20 mm Hg was imposed on the BBS. While the feedback parameters of $H_{AP\rightarrow STM}$, ie, K_p and K_i, were altered, the effect of the parameters on the AP response was investigated. Finally, the parameters that enabled the BBS to quickly and stably minimize the effect of P_d on AP were determined.

Efficacy of BBS in a Clinical Model of Transient Hypotension

The performance of the BBS was evaluated in a clinical model of rapid transient hypotension (n=21). Rapid hypotension was evoked by the sudden deflation of a thigh tourniquet, which is widely used to achieve bloodless dissection during total knee arthroplasty.[29–31] Acute hypotension immediately after tourniquet release is a well-

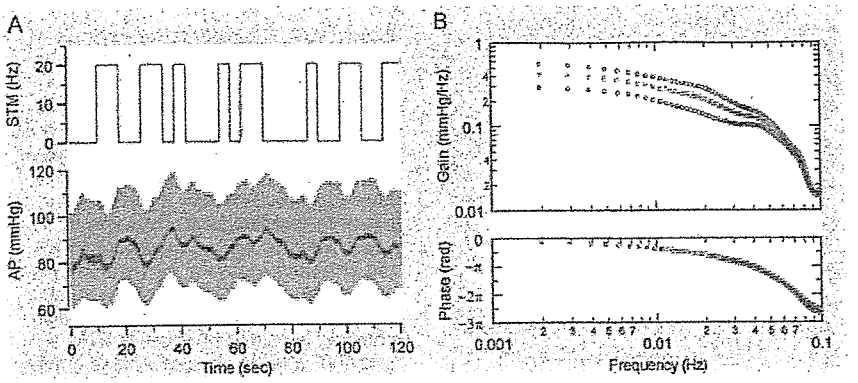

Figure 2. A, Representative example of time series data of the response of AP to random stimulation of the lower thoracic spinal cord. According to quasi-white noise, the STM was randomly altered between 0 and 20 Hz. The AP seems to slowly respond to STM with a delay. B, Transfer function of the AP response to the STM change. Data are expressed as mean±SD for 12 patients. rad indicates radians. See text for explanation.

known phenomenon that results from a rapid decrease in peripheral vascular resistance and an increase in venous pooling in the affected limb.[29] The degree of hypotension can be potentiated by the use of volatile anesthetic agents such as sevoflurane, which are central depressants of arterial baroreflex function.[32,33] Therefore, tourniquet-related hypotension during sevoflurane anesthesia can be used as a model of orthostatic hypotension in central baroreflex failure.

Briefly, a tourniquet was applied to the upper femur and inflated at 300 mm Hg for 60 minutes and then quickly deflated for 10 minutes. The procedure was then repeated. The BBS was activated during 1 of the 2 trials of tourniquet-related hypotension, and the electrical signals of STM, CVP, and AP were digitized at 100 Hz.

Statistical Analysis

The hemodynamic responses to tourniquet release were measured for each subject while the BBS was being activated and inactivated. The effects of the BBS execution on the hemodynamic changes at 10, 50, and 100 seconds after tourniquet release were analyzed by paired *t* tests with Bonferroni adjustment. Differences were considered significant at overall $P<0.05$.

Results

A representative example of original tracings of STM and AP during random stimulation of the spinal cord is shown in Figure 2A. Random on-off change in STM produced a delayed and slow change in AP. The relationship between STM and AP was quantitatively characterized by the frequency domain analysis (Figure 2B). The averaged transfer function from STM to AP, $H_{STM \rightarrow AP}$, had low-pass characteristics with a corner frequency of 0.06 Hz. The gain factor was 0.43 ± 0.13 mm Hg · Hz^{-1} at the steady state (lowest frequency) and gradually decreased with input frequency. The phase spectrum showed that the input-output relationship was in phase and that the phase delay increased toward higher frequencies. The squared coherence, a measure of linear dependence between STM and AP, was >0.9 in the frequency range of interest (data not shown).

The results of simulation for the design of the artificial vasomotor center, $H_{AP \rightarrow STM}$, are presented in Figure 3. The AP responses to the external disturbance P_d were simulated under 12 different combinations with feedback correction factors. Without feedback compensation, ie, when both feedback correction factors were zero, there was no attenuation of the effect of the external disturbance on AP. Therefore, AP fell by 20 mm Hg immediately after the imposition of P_d (Figure 3A, black line). By contrast, if either or both of the correction factors were too large, the underdamped oscillatory response of AP appeared, and the BBS became unstable. On the basis of these results, K_p was set at 1, and K_i was set at 0.1, so that the BBS could quickly and effectively attenuate the effect of the external disturbance (Figure 3B, red line).

A representative example of the results of the performance tests of the BBS is shown in Figure 4A. A sudden

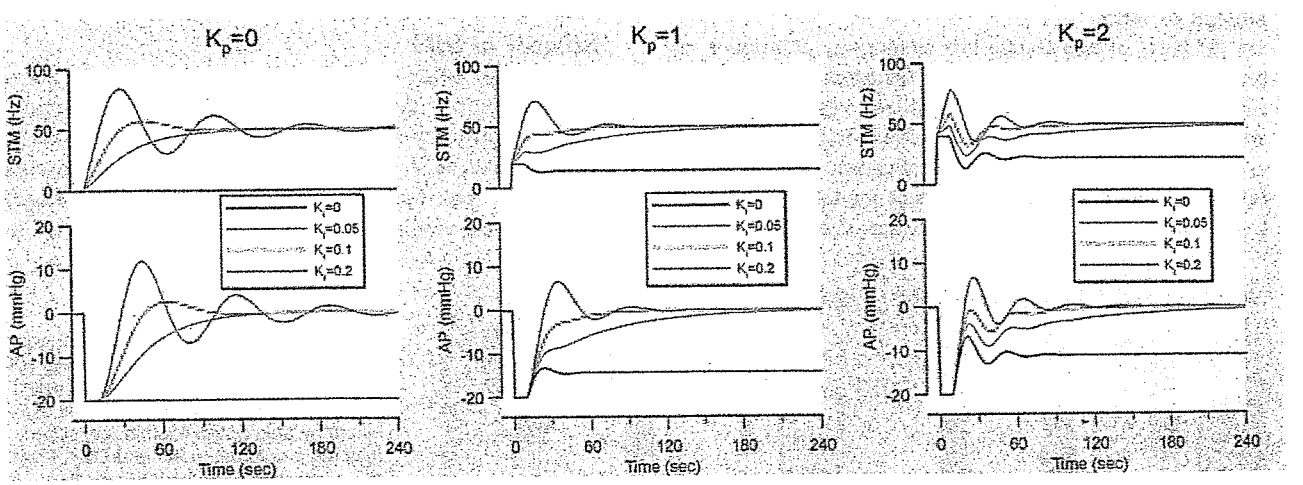

Figure 3. Numerical simulations of a feedback controller of the BBS. A stepwise pressure decline with an amplitude of 20 mm Hg is assumed to be imposed. Results are shown for 12 combinations of proportional (K_p) and integral (K_i) correction factors. See text for explanation.

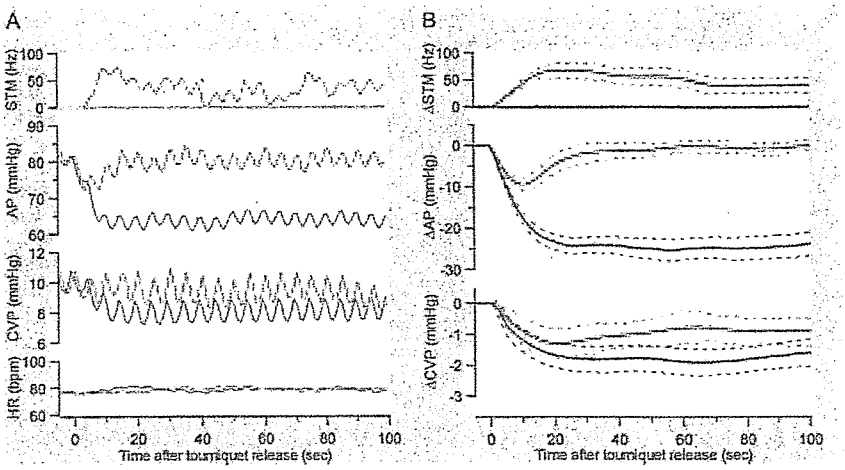

Figure 4. A, Representative example of original tracings of STM, AP, CVP, and heart rate (HR) during 2 episodes of rapid progressive hypotension induced by sudden deflation of a thigh tourniquet in a patient. When the BBS was inactive (blue line), AP decreased immediately after tourniquet release and did not return to baseline level. By contrast, when the BBS was activated (red line), the artificial vasomotor center automatically computed STM and drove an electrical stimulator to restore AP. B, Plots showing averaged changes in STM, AP, and CVP after tourniquet release among 21 patients. Data are expressed as mean (solid line)±SD (dotted line). See text for explanation.

deflation of the thigh tourniquet produced a rapid progressive fall in AP of ≈20 mm Hg within 10 seconds, while lowering CVP by 2 mm Hg. By contrast, when the BBS was activated, STM was computed automatically, and the spinal cord was stimulated appropriately to quickly and effectively attenuate the drop in AP and CVP. Figure 4B summarizes the results obtained from 21 patients, demonstrating effectiveness of the BBS performance in buffering the AP fall in response to the sudden release of the tourniquet. As demonstrated in Figure 5, tourniquet release resulted in an AP decrease of 17±3 mm Hg at 10 seconds, 25±2 mm Hg at 50 seconds, and 24±3 mm Hg at100 seconds. By contrast, during real-time execution of the BBS, the decrease in AP was 9±2 mm Hg at 10 seconds, 1±2 mm Hg at 50 seconds, and 0±1 mm Hg at 100 seconds after the deflation. These data indicated that the BBS significantly attenuated the decrease in AP at these 3 time points and nullified the hypotensive effect of tourniquet release within 50 seconds. Similarly, the BBS significantly suppressed the decrease in CVP within 50 seconds after the release of the tourniquet.

Discussion

Design of BBS

On the basis of knowledge and technology of bionics, we previously developed an artificial feedback control system for automatic regulation of sympathetic vasomotor tone in animal models of central baroreflex failure.[20–22] As a crucial first step to clinical application, we tested its feasibility and efficacy in a clinical model of orthostatic hypotension. A percutaneous epidural catheter approach was established for the monitoring of spinal function during surgery and for pain management,[28] and the lower thoracic level was selected for spinal cord stimulation based on earlier reports that the abdominal splanchnic vascular bed is a major effector mechanism for arterial baroreflex in animals[23,24] and humans.[25] Although the percutaneous epidural approach is less invasive than implantation surgery, spinal cord stimulation excites motor and sensory nerves[12,22,28] in addition to sympathetic vasomotor efferents. Therefore, administration of sufficient doses of muscle relaxants and analgesics was required during experimental protocols. Under these conditions, the dynamic response of AP to STM was easily characterized by the white noise system identification method. Furthermore, the quantitatively estimated results of transfer function analysis (Figure 2B) enabled simulation of the effects of feedback correction factors[27] on performance of the BBS. As demonstrated in Figure 3, the simulation results suggested that the specific combination of feedback correction factors could optimize the performance of the BBS. On the basis of these results, the feedback correction factors were determined to allow the BBS to quickly stabilize AP against the external disturbances.

Efficacy of BBS

The present study utilized a tourniquet-related model of hypotension[29–31] during general anesthesia[32,33] to approximate orthostatic hypotension due to central baroreflex failure. Except for the change in peripheral vascular resistance, the hemodynamic changes after tourniquet deflation are similar to those achieved after upright tilt-

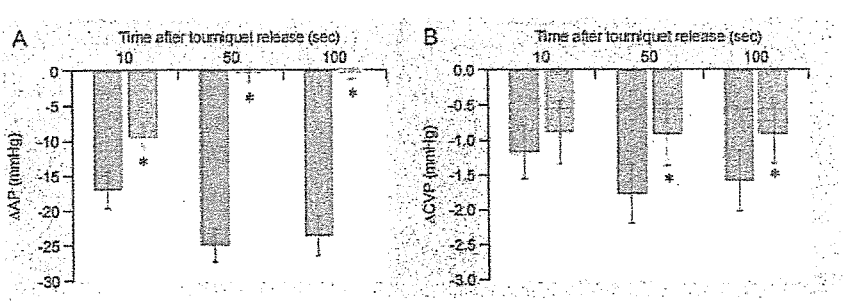

Figure 5. Bar graphs showing changes in AP (A) and CVP (B) at 10, 50, and 100 seconds after tourniquet release. Implementation of the BBS (red column) significantly attenuated tourniquet-related falls (blue column) in AP and CVP. Data are expressed as mean±SD for 21 patients. *Overall $P<0.05$.

ing.[29,31] For example, tourniquet release results in a rapid increase in venous pooling in the affected limb with a subsequent decrease in venous return and cardiac output. Under general anesthesia with volatile gases such as sevoflurane,[32,33] arterial baroreflex function is inhibited, and the hemodynamic disturbance produced by the tourniquet inevitably results in abrupt hypotension. In rare instances, tourniquet deflation can also trigger fatal circulatory collapse.[29]

Despite the fact that the BBS was implemented with fixed values of feedback correction factors for all patients, the BBS successfully stabilized AP against the hemodynamic challenge induced by sudden tourniquet release (Figure 4). These data indicate that the BBS may compensate for some individual differences in the dynamic response of AP to STM.

Finally, the CVP response to STM (Figure 4) in the present study suggests that the BBS attenuated a decrease in venous return. Previous studies have demonstrated that the baroreflex-mediated vasoconstriction in the splanchnic vascular bed is a major mechanism for recruitment of venous return during head-up tilting.[23,25] Therefore, the BBS may functionally mimic the baroreflex control of venous return and control of AP.

Study Limitations

This study possessed several limitations. First, based on the previous results[20–22] obtained from animal studies, the stimulation electrodes were placed in the epidural space at the level of the lower thoracic cord; however, further study to determine the optimal site of electrode placement would be of benefit. Second, it is unclear whether or not the feedback controller designed in the present study is universally applicable to other cases. Although preset parameters for feedback correction were used in the present study, other approaches based on a robust control theory could yield a better result. Finally, the epidural catheter method for sympathetic nerve stimulation is associated with significant pain and discomfort. Thus, practical use of the BBS requires an appropriate method for stimulating only efferent sympathetic nerves.

Clinical Implications

The present study confirmed the efficacy of the BBS in a clinical setting and suggests that the BBS has tremendous potential as a new therapeutic modality for treatment of severe orthostatic intolerance in patients with various syndromes of central baroreflex failure, including Shy-Drager syndrome, baroreceptor deafferentation, and traumatic spinal cord injuries.

Acknowledgments

This study was supported by a Health and Labor Sciences research grant (H14-NANO-002, H16-NANO-005, H15-KOKORO-019) from the Ministry of Health, Labor, and Welfare of Japan and by a grant-in-aid for scientific research (15300165) from the Ministry of Education, Science, Sports, and Culture of Japan.

Disclosures

None.

References

1. Guyton AC, Coleman TG, Granger HJ. Circulation: overall regulation. *Ann Rev Physiol.* 1972;34:13–46.
2. Robertson D. Diagnosis and management of baroreflex failure. *Primary Cardiol.* 1995;21:37–40.
3. Sunagawa K, Sato T, Kawada T. Integrative sympathetic baroreflex regulation of arterial pressure. *Ann N Y Acad Sci.* 2001;940:314–323.
4. Ketch T, Biaggioni I, Robertson R, Robertson D. Four faces of baroreflex failure: hypertensive crisis, volatile hypertension, orthostatic tachycardia, and malignant vagotonia. *Circulation.* 2002;105:2518–2523.
5. Sato T, Kawada T, Inagaki M, Shishido T, Takaki H, Sugimachi M, Sunagawa K. New analytical framework for understanding the sympathetic baroreflex control of arterial pressure. *Am J Physiol Heart Circ Physiol.* 1999;276:H2251–H2261.
6. Shy M, Drager GA. A neurological syndrome associated with orthostatic hypotension: a clinico-pathologic study. *Arch Neurol.* 1960;3:511–527.
7. The Consensus Committee of the American Autonomic Society and the American Academy of Neurology. Consensus statement on the definition of orthostatic hypotension, pure autonomic failure, and multiple system atrophy. *Neurology.* 1996;46:1470.
8. Schatz IJ. Farewell to the "Shy-Drager syndrome." *Ann Intern Med.* 1996;125:74–75.
9. Goldstein DS, Holmes C, Cannon RO III, Eisenhofer G, Kopin IJ. Sympathetic cardioneuropathy in dysautonomias. *N Engl J Med.* 1997;336:696–702.
10. Onrot J, Wiley RG, Fogo A, Biaggioni I, Robertson D, Hollister AS. Neck tumour with syncope due to paroxysmal sympathetic withdrawal. *J Neurol Neurosurg Psychiatry.* 1987;50:1063–1066.
11. Lee HT, Brown J, Fee WE Jr. Baroreflex dysfunction after nasopharyngectomy and bilateral carotid isolation. *Arch Otolaryngol Head Neck Surg.* 1997;123:434–437.
12. Frankel HL, Mathias CJ. Severe hypertension in patients with high spinal cord lesions undergoing electro-ejaculation: management with prostaglandin E_2. *Paraplegia.* 1980;18:293–299.
13. Matthews JM, Wheeler GD, Burnham RS, Malone LA, Steadward RD. The effects of surface anaesthesia on the autonomic dysreflexia response during functional electrical stimulation. *Spinal Cord.* 1997;35:647–651.
14. Wilcox CS, Puritz R, Lightman SL, Bannister R, Aminoff MJ. Plasma volume regulation in patients with progressive autonomic failure during changes in salt intake or posture. *J Lab Clin Med.* 1984;104:331–339.
15. Jordan J, Shannon JR, Diedrich A, Black B, Robertson D, Biaggioni I. Water potentiates the pressor effect of ephedra alkaloids. *Circulation.* 2004;109:1823–1825.
16. Kristinsson A. Programmed atrial pacing for orthostatic hypotension. *Acta Med Scand.* 1983;214:79–83.
17. Bannister R, da Costa DF, Hendry WG, Jacobs J, Mathias CJ. Atrial demand pacing to protect against vagal overactivity in sympathetic autonomic neuropathy. *Brain.* 1986;109:345–356.
18. Kachi T, Iwase S, Mano T, Saito M, Kunimoto M, Sobue I. Effect of L-threo-3,4-dihydroxyphenylserine on muscle sympathetic nerve activities in Shy-Drager syndrome. *Neurology.* 1988;38:1091–1094.
19. Obara A, Yamashita H, Onodera S, Yahara O, Honda H, Hasebe N. Effect of xamoterol in Shy-Drager syndrome. *Circulation.* 1992;85:606–611.
20. Sato T, Kawada T, Shishido T, Sugimachi M, Alexander J Jr, Sunagawa K. Novel therapeutic strategy against central baroreflex failure: a bionic baroreflex system. *Circulation.* 1999;100:299–304.
21. Sato T, Kawada T, Sugimachi M, Sunagawa K. Bionic technology revitalizes native baroreflex function in rats with baroreflex failure. *Circulation.* 2002;106:730–734.
22. Yanagiya Y, Sato T, Kawada T, Inagaki M, Tatewaki T, Zheng C, Kamiya A, Takaki H, Sugimachi M, Sunagawa K. Bionic epidural stimulation restores arterial pressure regulation during orthostasis. *J Appl Physiol.* 2004;97:984–990.
23. Hainsworth R, Karim F. Responses of abdominal vascular capacitance in the anaesthetized dog to changes in carotid sinus pressure. *J Physiol Lond.* 1976;262:659–677.

24. Carneiro JJ, Donald DE. Blood reservoir function of dog spleen, liver, and intestine. *Am J Physiol Heart Circ Physiol.* 1977;232:H67–H72.
25. Minson CT, Wladkowski SL, Pawelczyk JA, Kenney WL. Age, splanchnic vasoconstriction, and heat stress during tilting. *Am J Physiol Regul Integr Comp Physiol.* 1999;276:R203–R212.
26. Marmarelis PZ, Marmarelis VZ. *Analysis of Physiological Systems: The White-Noise Approach.* New York, NY: Plenum; 1978.
27. Kawada T, Sunagawa G, Takaki H, Shishido T, Miyano H, Miyashita H, Sato T, Sugimachi M, Sunagawa K. Development of a servo-controller of heart rate using treadmill. *Jpn Circ J.* 1999;63:945–950.
28. Shimoji K, Hokari T, Kano T, Tomita M, Kimura R, Watanabe S, Endoh H, Fukuda S, Fujiwara N, Aida S. Management of intractable pain with percutaneous epidural spinal cord stimulation: differences in pain-relieving effects among diseases and sites of pain. *Anesth Analg.* 1993;77:110–116.
29. Kahn RL, Marino V, Urquhart B, Sharrock NE. Hemodynamic changes associated with tourniquet use under epidural anesthesia for total knee arthroplasty. *Reg Anesth.* 1992;17:228–232.
30. Feldman DL, Wigod M, Barwick W, Levin LS. Tourniquet-related hypotension in venous stasis ulcer excision. *Ann Plast Surg.* 1993;30:556–559.
31. Sander-Jensen K, Mehlsen J, Secher NH, Bach FW, Bie P, Giese J, Schwartz TW, Trap-Jensen J, Warberg J. Progressive central hypovolaemia in man–resulting in a vasovagal syncope? Haemodynamic and endocrine variables during venous tourniquets of the thighs. *Clin Physiol.* 1987;7:231–242.
32. Tanaka M, Nishikawa T. Arterial baroreflex function in humans anaesthetized with sevoflurane. *Br J Anaesth.* 1999;82:350–354.
33. Keyl C, Schneider A, Hobbhahn J, Bernardi L. Sinusoidal neck suction for evaluation of baroreflex sensitivity during desflurane and sevoflurane anesthesia. *Anesth Analg.* 2002;95:1629–1636.

CLINICAL PERSPECTIVE

Central baroreflex failure due to Shy-Drager syndrome, baroreceptor deafferentation, and traumatic spinal cord injuries results in severe orthostatic hypotension. However, most commonly used interventions, such as salt loading, cardiac pacing, and pharmacological approaches, can neither restore nor reproduce the functioning of a native vasomotor center. Here, we proposed a novel therapeutic strategy against central baroreflex failure and developed a bionic baroreflex system (BBS). The BBS consisted of a pressure sensor, computer, electrical stimulator, and epidural catheter with sympathetic nerve stimulation electrodes. While automatically calculating the frequency of a pulse train in response to a change in arterial pressure, the computer drove the stimulator at the appropriate frequency to stabilize arterial pressure against an external disturbance. According to a parametric negative-feedback control theory, we designed an algorithm of the computer functioning as an artificial vasomotor center. The efficacy of the BBS was tested in a clinical model of orthostatic hypotension during knee joint surgery. Without the implementation of the BBS, a sudden deflation of a thigh tourniquet resulted in rapid progressive hypotension. By contrast, during real-time execution of the BBS, arterial pressure was quickly restored to the baseline level before tourniquet release. These results suggest the technical feasibility of functional restoration of arterial baroreflex with the BBS.

ELSEVIER

Cardiovascular Research 73 (2007) 794–805

Cardiovascular Research

www.elsevier.com/locate/cardiores

Soluble TNF receptors prevent apoptosis in infiltrating cells and promote ventricular rupture and remodeling after myocardial infarction

Yoshiya Monden [a], Toru Kubota [a,*], Takaki Tsutsumi [a], Takahiro Inoue [a], Shunichi Kawano [a], Natsumi Kawamura [a], Tomomi Ide [a], Kensuke Egashira [a], Hiroyuki Tsutsui [b], Kenji Sunagawa [a]

[a] *Department of Cardiovascular Medicine, Kyushu University Graduate School of Medical Sciences, 3-1-1 Maidashi, Higashi-ku, Fukuoka 812-8582, Japan*
[b] *Department of Cardiovascular Medicine, Hokkaido University Graduate School of Medicine, Kita-15, Nishi-7, Kita-ku, Sapporo 060-8638, Japan*

Received 7 September 2006; received in revised form 30 November 2006; accepted 19 December 2006
Available online 23 December 2006
Time for primary review 27 days

Abstract

Objective: Tumor necrosis factor (TNF)-α induced in damaged myocardium has been considered to be cardiotoxic. However, the negative results of RENEWAL and ATTACH prompt us to reconsider the role of TNF-α in cardiovascular diseases. The present study aimed to evaluate the effects of soluble TNF receptor treatment on myocardial infarction (MI).
Methods: An adenovirus encoding a 55-kDa TNF receptor-IgG fusion protein (AdTNFR1) was used to neutralize TNF-α, and an adenovirus encoding LacZ (AdLacZ) served as control. In the pre-MI treatment protocol, mice were given an intravenous injection of AdTNFR1 or AdLacZ 1 week before left coronary artery ligation to induce MI. In the post-MI treatment protocol, mice were treated with AdTNFR1 or AdLacZ 1 week after left coronary ligation.
Results: Treatment with AdTNFR1 neutralized bioactivity of TNF-α that was activated after MI and prevented apoptosis of infiltrating cells in infarct myocardium. However, pre-MI treatment with AdTNFR1 promoted ventricular rupture by reducing fibrosis with further activation of matrix metalloproteinase (MMP)-9. Post-MI treatment with AdTNFR1 exacerbated ventricular dysfunction and remodeling, with enhanced fibrosis of non-infarct myocardium with further MMP-2 activation.
Conclusions: Both pre- and post-MI treatments with AdTNFR1 were deleterious in a mouse MI model. Thus, TNF-α may play not only toxic but also protective roles in MI.

Keywords: Apoptosis; Cytokines; Infarction; Matrix metalloproteinases; Remodeling

1. Introduction

Tumor necrosis factor-α (TNF-α) is a proinflammatory cytokine that exerts a wide range of biological activities [1]. TNF-α is induced in the failing human heart [2], and considered to be cardiotoxic, because in vitro studies have shown that TNF-α suppresses cardiac contractility [3], provokes myocardial hypertrophy [4] and induces apoptosis in cardiac myocytes [5]. It also has direct effects on the matrix and collagen framework, and is a potential major contributor to cardiac remodeling [6,7]. However, in anti-cytokine clinical trials, the use of either a soluble TNF receptor (RENEWAL) [8] or an anti-TNF antibody (ATTACH) [9] was not beneficial to patients with heart failure. Especially, patients who received the high dose (10 mg/kg) of infliximab (anti-TNF antibody) were more likely to die or be hospitalized for heart failure than patients in the placebo group. High doses of anti-TNF antibodies might have exacerbated the clinical condition of patients with moderate-to-severe chronic heart failure. These results suggest that TNF-α may not be exclusively toxic but may be partially protective in cardiovascular diseases.

Accumulated evidence indicates that cytokines are important mediators of wound healing and remodeling after myocardial infarction (MI). However, the roles of these

* Corresponding author. Tel.: +81 92 642 5359; fax: +81 92 642 5374.
E-mail address: kubotat@cardiol.med.kyushu-u.ac.jp (T. Kubota).

0008-6363/$ - see front matter © 2006 European Society of Cardiology. Published by Elsevier B.V. All rights reserved.
doi:10.1016/j.cardiores.2006.12.016

cytokines in MI remain controversial. Blockade of these cytokines has been reported to be beneficial [10–13], deleterious [14,15], or bidirectional [16,17]. Therefore, the present study was designed to assess the role of TNF-α induction in the process of wound healing and cardiac remodeling after MI. We used soluble TNF receptors to block the bioactivity of TNF-α [18]. Our results indicated that treatment with soluble TNF receptors prevented apoptosis, but significantly promoted ventricular rupture and remodeling with further activation of matrix metalloproteinases (MMPs) after MI. These results support the hypothesis that TNF-α may play not only toxic but also protective roles in MI.

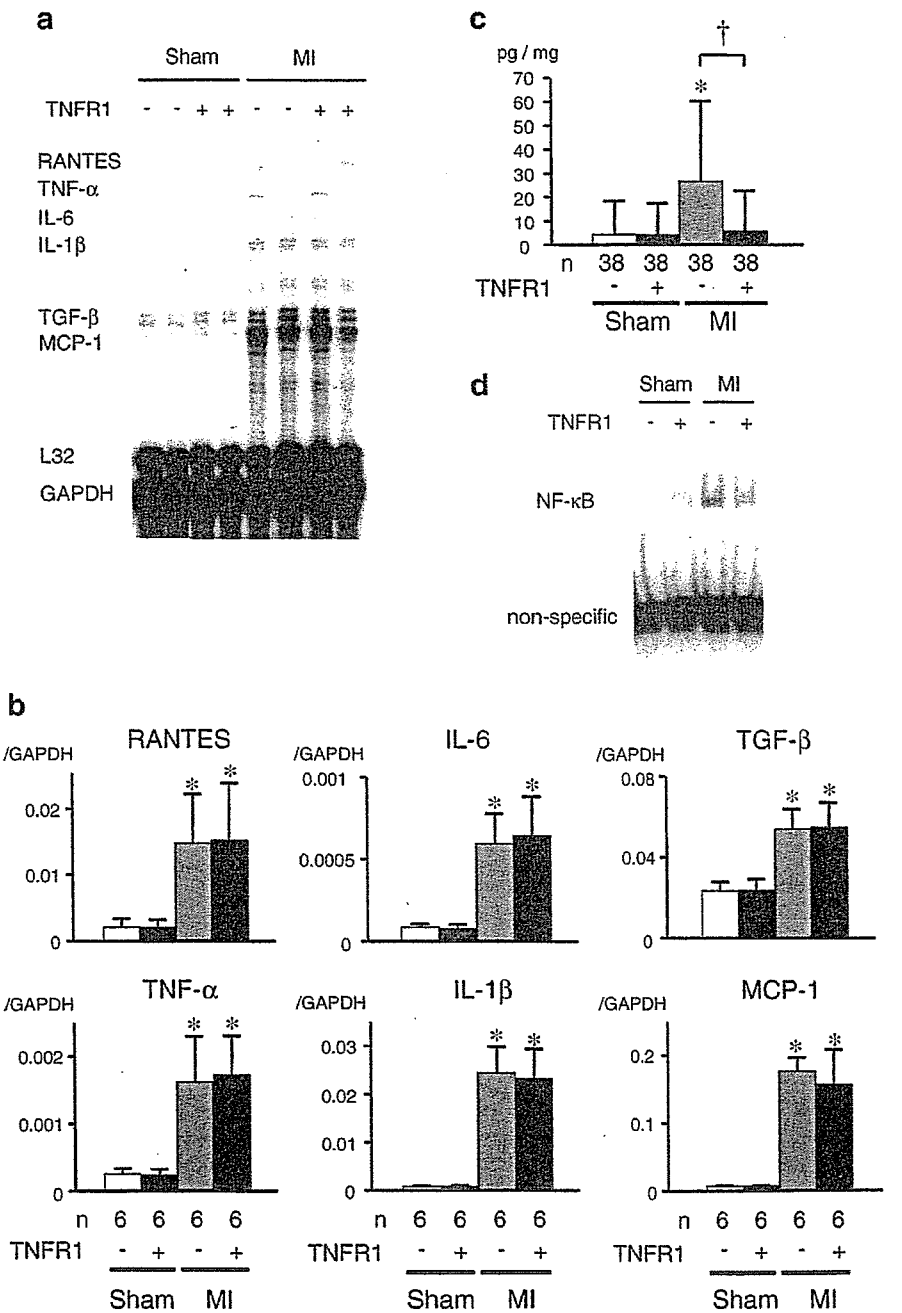

Fig. 1. Multi-probe RNase protection assay for proinflammatory cytokines and chemokines in infarct myocardium on day 3 after MI: a representative assay (a) and summarized data of densitometric analysis (b). Each value is normalized to that of GAPDH in each template set as an internal control. Cytotoxicity assay for TNF-α in infarct myocardium using WEHI cell line (c). Electrophoretic mobility shift assay for activation of NF-κB in infarct myocardium (d). Values are mean±SD. TNFR1 (−) indicates pre-MI treatment with AdLacZ; TNFR1 (+), pre-MI treatment with AdTNFR1; Sham, sham-operated mice; MI, coronary ligated mice. *$p<0.05$ vs. Sham/LacZ mice, †$p<0.05$ vs. MI/LacZ mice.

2. Methods

2.1. Animal model

An MI model was produced in male ICR mice (8–10 weeks old, weighing 35–40 g) by ligating the left coronary artery [10,16,19]. Sham operation without coronary artery ligation was also performed. This study was reviewed by the Committee of the Ethics on Animal Experiment, Kyushu University Graduate School of Medical Sciences and conducted in compliance with the Guideline for Animal Experiment of Kyushu University and the Japanese Law (No.105) and Notification (No. 6). The investigation conforms to the *Guide for the Care and Use of Laboratory Animals* published by the US National Institutes of Health (NIH Publication No. 85-23, revised 1996).

2.2. Experimental design

To block the activity of TNF-α, 10^9 pfu of replication-deficient recombinant adenovirus was used, which encodes the extracellular domain of the human 55-kDa TNF receptor (soluble TNFR1) coupled with a mouse IgG heavy chain (AdTNFR1), and has been proven to suppress myocardial inflammation secondary to TNF-α overexpression in our previous study [18]. An adenovirus encoding LacZ (AdLacZ) served as control. To determine the effects of soluble TNF receptors on early ventricular rupture and late remodeling after MI, two independent protocols were performed. In the pre-MI treatment protocol, four experimental groups were studied: Sham/LacZ (n=63), Sham/TNFR1 (n=63), MI/LacZ (n=155), and MI/TNFR1 (n=161). AdTNFR1 or AdLacZ was injected intravenously 1 week before left coronary artery ligation, and the effects of TNF-α blockade on early ventricular rupture were examined on days 1, 3 and 14 after MI. In the post-MI treatment protocol, four experimental groups were studied: Sham/LacZ (n=19), Sham/TNFR1 (n=18), MI/LacZ (n=36), and MI/TNFR1 (n=38). AdTNFR1 or AdLacZ was injected intravenously 1 week after left coronary artery ligation, and the effects of TNF-α blockade on late remodeling were examined on day 28 after MI. For both protocols, the mice were randomly assigned independently to the four experimental groups. Due to the high mortality in MI groups, the number of MI mice used was 2–3 times greater than the number of Sham mice.

Table 1
Characteristics of animal models (day 3)

	Sham/LacZ (n=16)	Sham/TNFR1 (n=15)	MI/LacZ (n=25)	MI/TNFR1 (n=26)
Echocardiographic data (under anesthesia)				
Heart rate (bpm)	486±26	485±24	490±17	487±13
LV EDD (mm)	3.4±0.1	3.3±0.2	3.8±0.4*	3.9±0.3*
LV ESD (mm)	2.2±0.1	2.1±0.1	3.1±0.4*	3.2±0.3*
Fractional shortening (%)	34.1±1.9	35.2±1.5	19.2±3.3*	17.6±2.3*
Infarct wall thickness (mm)	–	–	0.63±0.09	0.64±0.08
Non-infarct wall thickness (mm)	0.81±0.04	0.81±0.04	0.82±0.04	0.80±0.03
Hemodynamic data (tail-cuff system, awake)				
Heart rate (bpm)	630±53	623±54	635±86	636±92
Systolic blood pressure (mm Hg)	112±8	113±7	103±11	103±11
Organ weight data				
Body wt (g)	38.0±1.4	37.4±2.0	33.5±2.0*	33.0±2.5*
Lung wt/Body wt (mg/g)	5.17±0.33	5.28±0.24	7.83±2.52*	7.56±1.92*
Pleural effusion (%)	0	0	20.0	19.2
N			12	12
Infarct area (%)	–	–	53.1±4.3	54.7±3.8

LV, left ventricular; EDD, end-diastolic diameter; ESD, end-systolic diameter; wt, weight. Values are mean±SD. *P<0.05 vs. Sham/LacZ.

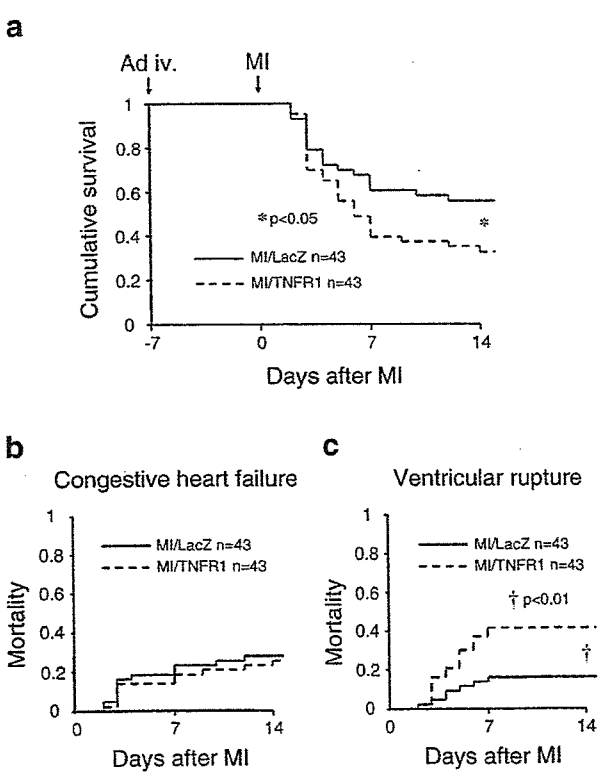

Fig. 2. Kaplan–Meier survival curves of coronary ligated mice with or without pre-MI TNFR1 treatment (a). Mortality of coronary ligated mice from congestive heart failure (b) and ventricular rupture (c). *p<0.05 vs. MI/LacZ mice, †p<0.01 vs. MI/LacZ mice.

2.3. Enzyme-linked immunosorbent assay (ELISA)

Human TNFR1 protein levels were assessed by ELISA (Quantikine, No. DRT100, R&D Systems) [18].

2.4. RNase protection assay (cytokine gene expression)

Multi-probe RNase protection assays (RPA) were performed according to the manufacture's protocol (RiboQuant,

Table 2
Characteristics of animal models (day 14)

	Sham/LacZ (n=9)	Sham/TNFR1 (n=10)	MI/LacZ (n=24)	MI/TNFR1 (n=14)
Echocardiographic data (under anesthesia)				
Heart rate (bpm)	466±15	463±14	459±47	469±55
LV EDD (mm)	3.4±0.3	3.4±0.3	5.5±0.3*	5.5±0.4*
LV ESD (mm)	2.2±0.3	2.3±0.3	4.8±0.3*	4.8±0.4*
Fractional shortening (%)	34.6±2.1	34.4±2.1	12.5±2.1*	13.4±3.0*
Infarct wall thickness (mm)	–	–	0.27±0.05	0.24±0.05
Non-infarct wall thickness (mm)	0.80±0.00	0.79±0.04	0.93±0.08*	0.88±0.08*
Organ weight data				
Body wt (g)	39.5±1.7	38.1±2.5	37.3±3.7	35.7±3.7*
Lung wt/Body wt (mg/g)	5.16±0.32	5.39±0.39	10.31±4.00*	9.89±2.77*
Pleural effusion (%)	0	0	95.5	100
Infarct area (%)	–	–	58.6±2.2	57.5±1.6

LV, left ventricular; EDD, end-diastolic diameter; ESD, end-systolic diameter; wt, weight. Values are mean±SD. *P<0.05 vs. Sham/LacZ.

PharMingen, San Diego, California, USA) using a custom template set containing probes for murine RANTES, TNF-α, IL-6, IL-1β, TGF-β, monocyte chemotactic protein-1(MCP-1), L32, and GAPDH (No. 557310) [10,16,18].

2.5. Determination of tissue TNF-α bioactivity

Myocardial TNF-α bioactivity was measured with a cytotoxicity assay using the TNF-sensitive WEHI murine fibrosarcoma cell line [11].

2.6. Electrophoretic mobility shift assay (EMSA)

Activation of NF-κB was evaluated by the electrophoretic mobility shift assay (EMSA) according to the manufacture's instructions (Gel Shift Assay System E3300, Promega, Madison, Wisconsin, USA) [20]. Nuclear protein was isolated from the myocardium as previously reported [20]. Samples were resolved on a 5% acrylamide gel in 0.25% Tris–borate–EDTA buffer.

2.7. Echocardiographic and hemodynamic measurements

Echocardiographic studies were performed using an ultrasonographic system (ALOKA SSD-5500; Tokyo, Japan) as previously described [10,16,19]. In the pre-MI treatment protocol, arterial blood pressure and heart rate were also measured awake on day 3 with the use of a noninvasive tail–cuff system (BP-98A, Softron). In the post-MI treatment protocol, a 1.4 Fr micromanometer-tipped catheter (Millar) was inserted into the left ventricle (LV) through the right carotid artery to measure LV pressure on day 28 under anesthesia with 2.5% Avertin (14 μl/g body weight, IP, Aldrich Chemical Co) [10,16,19].

2.8. Infarct size and pathological analysis

Infarct size was determined by methods described previously for mice [10,16,19]. Briefly, the LV was cut from apex to base into 4 transverse sections. Infarct length was measured along the endocardial and epicardial surfaces from each of the LV sections, and the values from all specimens were summed. Total LV circumference was calculated as the sum of endocardial and epicardial segment lengths from all LV sections. Infarct size (in percent) was calculated as total infarct circumference divided by total LV circumference. Picrosirius red staining was performed to observe interstitial collagen fibers and determine collagen volume fraction [10,19]. Collagen volume fraction was measured at 6 fields for each heart. Myocardial infiltration was quantified by determining nuclear density (nuclei/mm^2) on hematoxylin and eosin stained sections [18]. Because it is difficult to differentiate inflammatory cells from myocytes and/or fibroblasts, all nuclei were included. In each mouse, six independent high-power fields were analyzed and averaged. To further determine the number of macrophages, an immunohistochemical analysis using a specific antibody against mouse Mac-3 (macrophage marker, BD Pharmingen) was performed.

2.9. Apoptosis

Apoptosis was evaluated by a ligation-mediated PCR fragmentation (DNA laddering) assay (Maxim Biotech Inc) [20]. In addition, LV tissue sections were stained for terminal deoxynucleotidyl transferase-mediated dUTP nick end-labeling (TUNEL) to detect apoptotic cell [20]. The number of TUNEL-positive nuclei was counted, and the data were normalized per total nuclei identified as hematoxylin-positive staining in the same sections.

2.10. MMP zymography

Gelatin zymography was performed as previously described [19]. The zymograms were digitized, and the size-fractionated bands, which indicated the MMP proteolytic levels, were measured as the integrated optical density in a rectangular region of interest.

2.11. Double immunohistochemical staining for MMP-9 and Mac-3

Double immunohistochemical staining for MMP-9 (Santa Cruz Biotech.) and Mac-3 (macrophage marker, BD Pharmingen) in infarct myocardial sections were performed by routine protocols at our laboratory to localize MMP-9 with potential MMP-producing cells [21].

2.12. Statistical analysis

The results are presented as mean±SD. Statistical comparisons were performed using ANOVA with Students–Newman–

Keuls post hoc test or unmatched Student's *t*-test where appropriate. When the Levene test for homogeneity of variance revealed significant differences between groups, nonparametric tests (Kruskal–Wallis, the Mann–Whitney *U* test) were performed on the variables. Survival analysis was performed by the Kaplan–Meier method, and between-group difference in survival was tested by the log-rank test. Differences were considered significant at a p value less than 0.05.

3. Results

3.1. Pre-MI treatment protocol

3.1.1. TNF-α in infarct myocardium

Plasma levels of human TNFR1 10 days after inoculation with AdTNFR1 (or 3 days after MI or sham operation) were 512.7±93.6 (SD) μg/ml, which were similar to our previous report [18]. Multi-probe RPA was used to evaluate expression of proinflammatory cytokines and chemokines in infarct myocardium 3 days after MI or sham operation (Fig. 1a). Transcript levels of TNF-α, IL-1β, IL-6, TGF-β, MCP-1, and RANTES were significantly up-regulated in infarct myocardium, and were not affected by treatment with TNFR1 (Fig. 1b). However, as summarized in Fig. 1c, cytotoxic activity of TNF-α, which was significantly increased in infarct myocardium, was significantly attenuated by treatment with TNFR1. To examine the downstream signals of TNF-α, activation of NF-κB was evaluated in infarct myocardium on day 3 using EMSA. As shown in Fig. 1d, increased activation of NF-κB in infarct myocardium was attenuated by TNFR1 treatment (n=4 per group).

3.1.2. Increased ventricular rupture with TNFR1 treatment

Survival analysis was performed in four groups of mice, including Sham/LacZ, Sham/TNFR1, MI/LacZ, and MI/TNFR1. Mice that died within 12 h after the operation were excluded, because early operative mortality was not different between MI/LacZ (23.2%) and MI/TNFR1 mice (21.8%). No mice died after sham operation. In contrast, as shown in Fig. 2a, 19 of 43 MI/LacZ and 29 of 43 MI/TNFR1 mice died by the end of 2 weeks after coronary ligation. Statistical analysis indicated that pre-MI treatment with soluble TNF

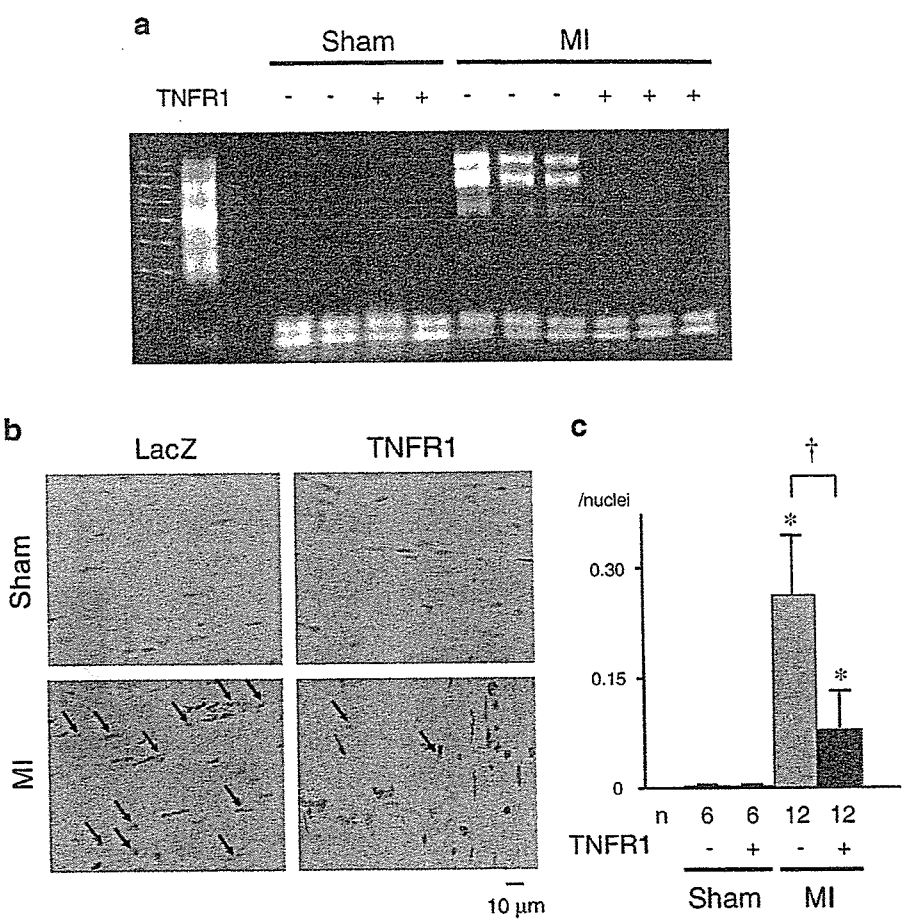

Fig. 3. Apoptosis assay in infarct myocardium on day 3 after MI: DNA laddering assay image (a), representative images of TUNEL staining (b), and summarized data for density of TUNEL-positive cells (c). Values are mean±SD. Arrows indicate TUNEL-positive cells; TNFR1 (−), pre-MI treatment with AdLacZ; TNFR1 (+), pre-MI treatment with AdTNFR1; Sham, sham-operated mice; MI, coronary ligated mice. *p<0.05 vs. Sham/LacZ mice, †p<0.05 vs. MI/LacZ mice.

receptors significantly increased the mortality after MI ($p<0.05$). The cause of death was classified as either congestive heart failure or ventricular rupture, because no mice died without congestion (pleural effusion and increased lung weight) or blood clot in the pericardial sac. Although mortality presumably due to congestive heart failure was not different between MI/LacZ and MI/TNFR1 mice (Fig. 2b), mortality due to ventricular rupture was significantly higher in MI mice treated with TNFR1 (Fig. 2c). To elucidate the mechanisms by which pre-MI TNFR1 treatment promotes ventricular rupture, the following studies were performed.

3.1.3. No differences in hemodynamic parameters or infarct size

Hemodynamic parameters and infarct size on days 3 and 14 after MI are summarized in Tables 1 and 2, respectively. Echocardiography revealed that both end-diastolic and end-systolic dimensions as well as non-infarct wall thickness increased progressively after MI, with significant decreases in fractional shortening and infarct wall thickness. These changes in echocardiographic parameters were not affected by treatment with TNFR1. Furthermore, infarct size was similar in MI/LacZ and MI/TNFR1 mice. Because neither

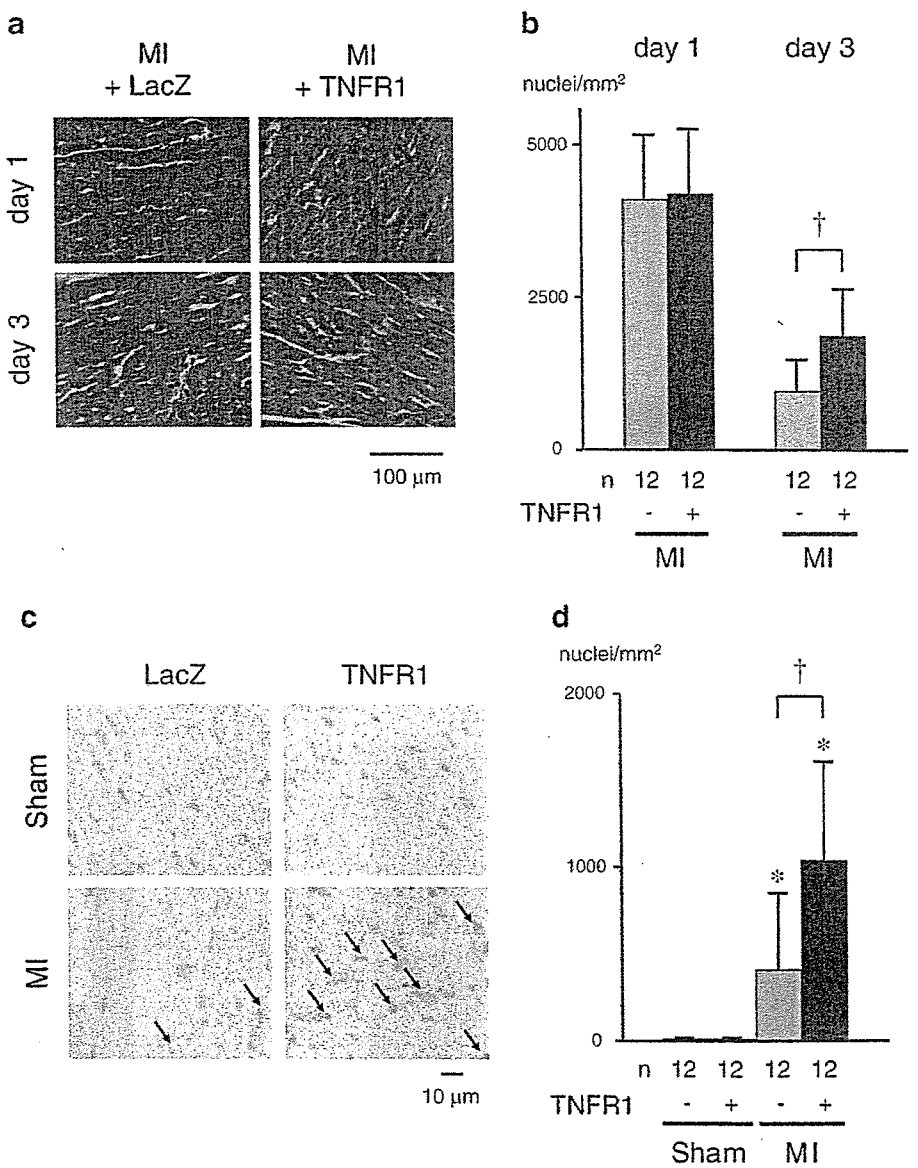

Fig. 4. Pathological analysis of the infarct myocardium: representative micrographs of hematoxylin–eosin staining (a), summarized data for total cell density on days 1 and 3 after MI (b), representative micrographs of immunohistochemical staining for mouse Mac-3 (c), and summarized data for density of Mac-3-positive cells on day 3 after MI (d). Values are mean±SD. Arrows indicate Mac-3-positive cells; TNFR1 (−), pre-MI treatment with AdLacZ; TNFR1 (+), pre-MI treatment with AdTNFR1; Sham, sham-operated mice; MI, coronary ligated mice. *$p<0.05$ vs. Sham/LacZ mice, †$p<0.05$ vs. MI/LacZ mice.

heart rate nor systemic blood pressure was affected by TNFR1 treatment, increased ventricular rupture in MI/TNFR1 mice was not attributable to increased afterload or wall stress.

3.1.4. Reduced apoptosis and retention of infiltrating macrophages

DNA laddering assay indicated that apoptosis, which increased substantially in infarct myocardium, was markedly decreased by TNFR1 treatment (Fig. 3a). TUNEL staining was performed to identify apoptotic cells on day 3. TUNEL-positive cells were mostly infiltrating mononuclear cells besides neutrophils and myocytes (Fig. 3b). As summarized in Fig. 3c, treatment with TNFR1 significantly reduced TUNEL-positive cells in infarct myocardium.

Hematoxylin and eosin staining was performed to evaluate infiltration of inflammatory cells. Marked infiltration of inflammatory cells was observed in infarct myocardium

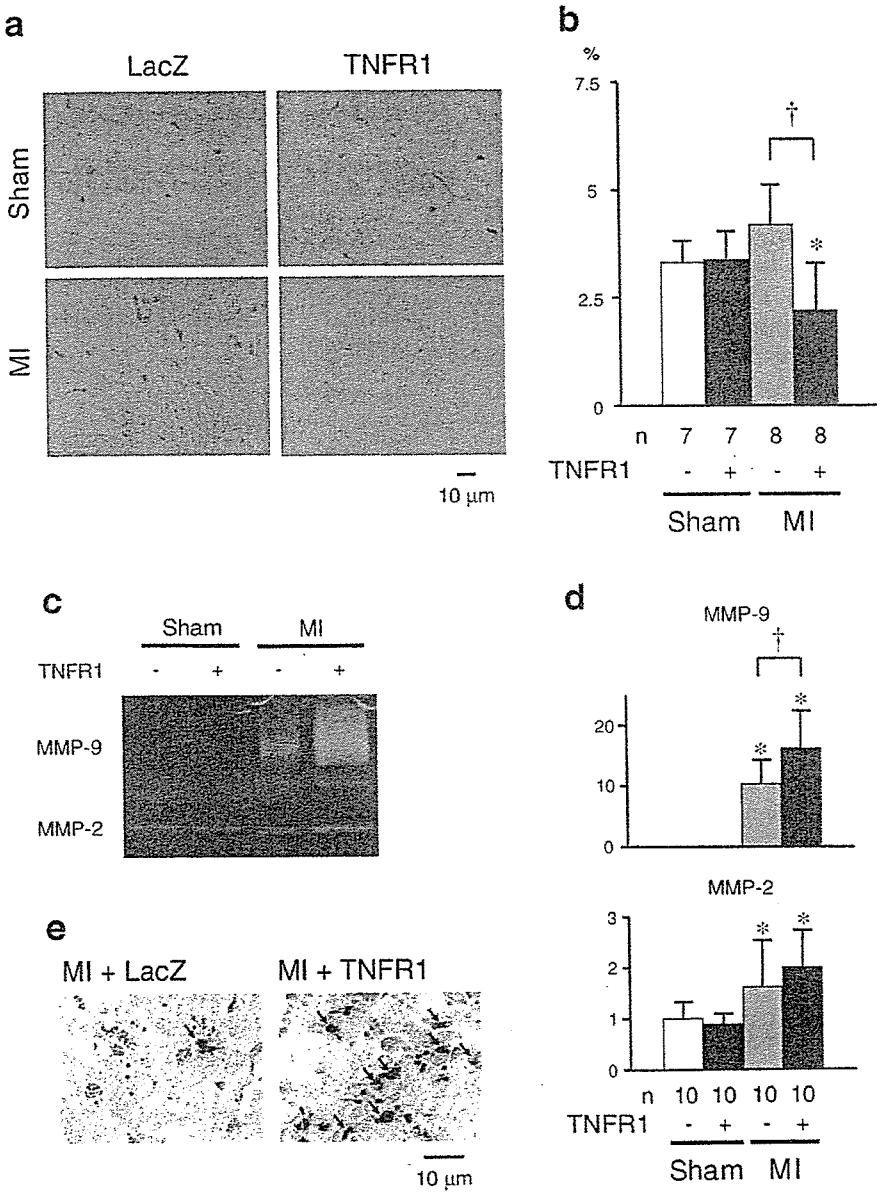

Fig. 5. Collagen volume analysis of the infarct myocardium on day 3 after MI: representative micrographs of Picrosirius red staining (a) and summarized data for collagen volume fraction (b). Gelatin zymography for MMP-2 and MMP-9 in infarct myocardium on day 3 after MI: representative gel (c) and summarized data for densitometric analysis (d). Each value is expressed as the ratio to the average of MMP-2 in Sham/LacZ mice. Double immunohistochemical staining for mouse Mac-3 and MMP-9 in infarct myocardium on day 3 after MI (e). Values are mean±SD. Arrows indicate both Mac-3- and MMP-9-positive cells; TNFR1 (−), pre-MI treatment with AdLacZ; TNFR1 (+), pre-MI treatment with AdTNFR1; Sham, sham-operated mice; MI, coronary ligated mice. *$p<0.05$ vs. Sham/LacZ mice, †$p<0.05$ vs. MI/LacZ mice.

on day 1, and subsequently subsided on day 3 (Fig. 4a). Although inflammatory cell infiltration was not significantly different between MI/LacZ and MI/TNFR1 mice on day 1, significantly more infiltrating cells remained in MI/TNFR1 myocardium on day 3, which might reflect reduced apoptosis by TNFR1 treatment (Fig. 4b). Immunohistochemical staining revealed that most of these retained infiltrating cells on day 3 were macrophages (Fig. 4c). As summarized in Fig. 4d, TNFR1 treatment significantly increased the number of macrophages in infarct myocardium on day 3.

3.1.5. Degradation of extracellular matrix with further activation of MMP-9

Collagen was visualized in LV cross-section using Picrosirius red staining (Fig. 5a). Collagen volume fraction was not affected by MI, but was significantly reduced in MI/TNFR1 mice on day 3 (Fig. 5b).

To further elucidate the mechanisms of reduced myocardial fibrosis in MI/TNFR1 mice, the activities of MMP-2 and -9 were evaluated in infarct myocardium on day 3 using gelatin zymography (Fig. 5c). The activities of MMP-2 and -9 increased significantly after MI (Fig. 5d). Treatment with soluble TNF receptors did not affect MMP-2 but significantly further activated MMP-9. Immunohistochemical staining identified macrophages as one of the major sources of MMP-9 in infarct myocardium (Fig. 5e).

Taken together, these results suggest that pre-MI treatment with TNFR1 prevents apoptosis of infiltrating cells in infarct myocardium, resulting in the retention of macrophages and further activation of MMP-9, which may further degrade and finally rupture the infarct myocardium.

3.2. Post-MI treatment protocol

3.2.1. Exacerbation of cardiac dysfunction and remodeling after MI

Post-MI treatment protocol was conducted to evaluate effects of TNFR1 on ventricular remodeling, because pre-MI treatment significantly increased ventricular rupture and precluded late phase analysis. In this study, 102 mice underwent coronary ligation, and 28 died within 7 days. The surviving mice ($n=74$) were randomly assigned to AdLacZ or AdTNFR1 injection on day 7. Four of 36 MI/LacZ and 9 of 38 MI/TNFR1 mice died of congestive heart failure by the end of 4 weeks after ligation (Fig. 6, $p=0.16$). None of the sham-operated mice died. Plasma levels of human TNFR1 3 weeks after inoculation with AdTNFR1 (or 4 weeks after MI or sham operation) were 71.1±28.5 (SD) μg/ml, which were similar to our previous report [18]. Percent infarct area was not different between MI/LacZ and MI/TNFR1 mice on day 28 (Table 3).

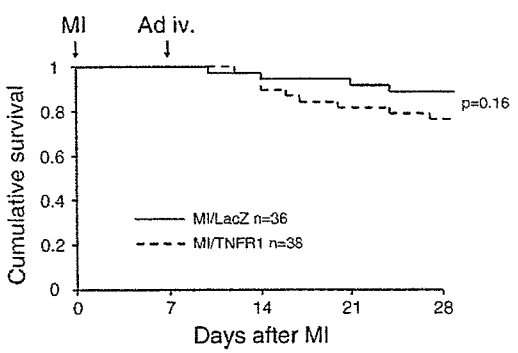

Fig. 6. Kaplan–Meier survival curves of coronary ligated mice with or without TNFR1 post-MI treatment.

Table 3
Characteristics of animal models (day 28)

	Sham/ LacZ	Sham/ TNFRI	MI/ LacZ	MI/ TNFR1
Echocardiographic data (under anesthesia)				
N	19	18	32	29
Heart rate (bpm)	465±11	461±13	471±16	467±14
LV EDD (mm)	3.9±0.3	4.0±0.3	5.6±0.3*	6.0±0.4*†
LV ESD (mm)	2.5±0.2	2.6±0.2	4.8±0.2*	5.3±0.5*†
Fractional shortening (%)	35.6±1.4	35.7±1.9	14.1±0.9*	11.7±1.9*†
Infarct wall thickness (mm)	–	–	0.29±0.03	0.29±0.03
Non-infarct wall thickness (mm)	0.78±0.04	0.76±0.05	0.95±0.06*	1.06±0.07*†
Hemodynamic data (Millar catheter; under anesthesia)				
N	6	6	12	11
Heart rate (bpm)	434±21	435±22	429±25	434±24
Mean aortic pressure (mm Hg)	81.8±4.3	80.5±4.6	78.3±4.3	79.2±4.5
LV EDP (mm Hg)	2.1±0.9	2.1±1.0	10.1±2.5*	14.5±3.3*†
LV$dP/dt_{max}$ (mm Hg/s)	7243±424	7084±422	5363±794*	4482±568*†
LV$dP/dt_{min}$ (mm Hg/s)	5047±274	4944±264	3864±602*	3219±424*†
Organ weight data				
N	19	18	32	29
Body wt (g)	42.0±2.1	41.9±2.4	40.7±2.5	40.6±3.1
Lung wt/Body wt (mg/g)	4.88±0.30	4.84±0.26	8.50±2.70*	10.13±2.78*†
Pleural effusion (%)	0	0	71.9	93.1
N	13	12	20	18
LV wt/Body wt (mg/g)	2.68±0.14	2.64±0.17	3.07±0.22*	3.33±0.29*†
N			12	11
Infarct area (%)	–	–	57.8±3.1	56.0±3.4*

LV, left ventricular; EDD, end-diastolic diameter; ESD, end-systolic diameter; EDP, end-diastolic pressure; wt, weight. Values are mean±SD. *$P<0.05$ vs. Sham/LacZ, †$P<0.05$ vs. MI/LacZ.

Echocardiography showed that cardiac dimensions of surviving mice on day 28 were significantly higher in MI/LacZ mice compared to Sham/LacZ or Sham/TNFR1 (Table 3). MI/TNFR1 mice showed significantly more cavity dilatation with exacerbation of contractile dysfunction compared with MI/LacZ. Pressure measurement with a Millar catheter showed no significant differences in heart rate and aortic blood pressure among 4 groups. However, LV end-diastolic pressure, which increased significantly in MI/LacZ mice, was further

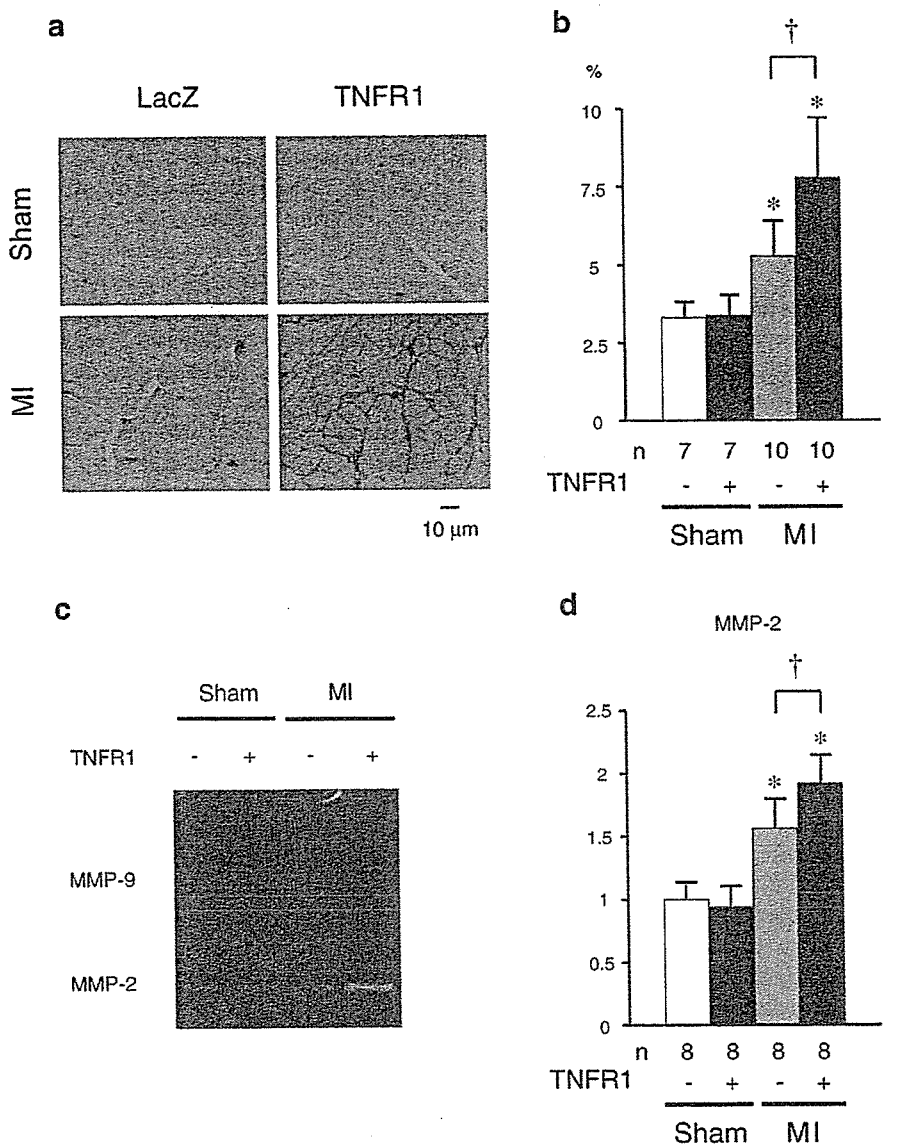

Fig. 7. Collagen volume analysis of the non-infarct myocardium on day 28 after MI: representative micrographs of Picrosirius red staining (a) and summarized data for collagen volume fraction (b). Gelatin zymography for MMP-2 and MMP-9 in non-infarct myocardium on day 28 after MI: representative gel (c) and summarized data for densitometric analysis (d). Each value is expressed as the ratio to the average of MMP-2 in Sham/LacZ mice. Values are mean±SD. TNFR1 (−) indicates post-MI treatment with AdLacZ; TNFR1 (+), post-MI treatment with AdTNFR1; Sham, sham-operated mice; MI, coronary ligated mice. *$p<0.05$ vs. Sham/LacZ mice, †$p<0.05$ vs. MI/LacZ mice.

augmented significantly in MI/TNFR1 mice. Both LV dP/dt_{max} and LV dP/dt_{min}, which decreased significantly in MI, were further lowered significantly by post-MI treatment with soluble TNF receptors. Although body weight was similar among 4 groups, LV weight/body weight ratio increased significantly in MI and further exacerbated with TNFR1 treatment. Along with increased LV end-diastolic pressure, lung weight/body weight ratio also increased significantly in MI/LacZ mice with further increment by TNFR1 treatment. These results suggest that the post-MI treatment with soluble TNF receptors exacerbates ventricular remodeling and pulmonary congestion after MI.

3.2.2. Enhanced fibrosis in non-infarct myocardium with further activation of MMP-2

Collagen was visualized in LV cross-section using Picrosirius red staining (Fig. 7a). As summarized in Fig. 7b, collagen volume fraction, which increased in non-infarct myocardium of MI/LacZ mice, was further augmented significantly by TNFR1 treatment. To further elucidate the mechanisms of increased myocardial fibrosis in MI/TNFR1 mice, MMP-2 and -9 activities were evaluated in non-infarct myocardium on day 28 using gelatin zymography (Fig. 7c). As summarized in Fig. 7d, MMP-2 activity increased significantly

after MI and was further activated by TNFR1 treatment, although MMP-9 activity was not altered.

These results indicate that post-MI treatment with soluble TNF receptors exacerbates ventricular dysfunction and remodeling, with enhanced fibrosis and further activation of MMP-2 in non-infarct myocardium.

4. Discussion

Proinflammatory cytokines including TNF-α have been implicated in the pathogenesis of cardiovascular diseases [6,7]. However, the roles of these cytokines in myocardial infarction remain controversial. In the present study, we evaluated the effects of soluble TNF receptor treatment on MI. Treatment with soluble TNFR1 neutralized the bioactivity of TNF-α that was activated after MI, and prevented apoptosis of infiltrating cells in the infarct myocardium. However, pre-MI treatment with soluble TNFR1 promoted ventricular rupture by reducing fibrosis with further activation of MMP-9. Furthermore, post-MI treatment with soluble TNFR1 exacerbated ventricular dysfunction and remodeling, and enhanced fibrosis in non-infarct myocardium with further activation of MMP-2. Because both pre- and post-MI treatments with soluble TNFR1 were deleterious in a mouse model of MI, TNF-α may play some protective roles in MI.

We used AdTNFR1 to block the effects of TNF-α after MI. We have previously confirmed the efficacy of AdTNFR1 treatment in transgenic mice with cardiac-specific overexpression of TNF-α [18]. Injection of 10^9 pfu of AdTNFR1 increased plasma levels of soluble TNFR1 substantially and ameliorated myocardial inflammation induced by TNF-α overexpression for 6 weeks [18]. In the present study, pro-inflammatory cytokines and chemokines including TNF-α, IL-1β, IL-6, TGF-β, MCP-1, and RANTES were up-regulated in infarct myocardium 3 days after coronary ligation. Pre-MI treatment with AdTNFR1 increased plasma levels of soluble TNFR1 as previously reported [18]. Although AdTNFR1 treatment did not affect the transcript levels of proinflammatory cytokines and chemokines, it significantly blocked the bioactivity of TNF-α in infarct myocardium. These results indicate that treatment with AdTNFR1 neutralizes the effects of TNF-α induced after MI. Furthermore, induction of proinflammatory cytokines and chemokines in infarct myocardium is not solely mediated by TNF-α.

Cardiac rupture is an acute fatal complication that occurs during the early phase after MI. Disorganized infarct healing and the resultant deficiency or disruption of extracellular matrix (ECM) at the infarction site may lead to myocardial rupture. In the present study, we have shown that pre-MI treatment with soluble TNFR1 increases ventricular rupture after MI without affecting systemic blood pressure or heart rate, but significantly reduced collagen content of infarct myocardium with further MMP-9 activation. Because targeted disruption of MMP-9 is known to prevent ventricular rupture after MI [22], further activation of MMP-9 may be the primary cause of increased ventricular rupture in this mouse MI model. Further activation of MMP-9 may be attributed to increased macrophages in soluble TNFR1-treated infarct myocardium, because macrophages produce substantial amounts of MMP-9 [21]. Increased macrophages may result from the anti-apoptotic effects of soluble TNFR1, because apoptosis of infiltrating cells was significantly attenuated by the treatment. These results suggest that TNF-α may be necessary for proper coordination of tissue repair processes after MI.

TNF-α is a potent inducer of apoptosis in a variety of cells including macrophages and myocytes [5,20]. In the present study, we have demonstrated that treatment with soluble TNFR1 decreases the number of apoptotic cells in infarct myocardium 3 days after MI, which is consistent with the blockade of TNF-α bioactivity by the treatment. Most of the apoptotic cells were interstitial infiltrating cells including macrophages, rather than myocytes. Because the number of infiltrating cells was not different between AdLacZ- and AdTNFR1-treated infarct myocardium 1 day after MI, the increase in relative number of macrophages in AdTNFR1-treated infarct myocardium after 3 days was probably due to decreased apoptosis of infiltrating cells. In contrast, Kurrelmeyer et al. [15] reported that targeted disruption of both TNFR1 and TNFR2 increased the size of infarct myocardium by enhancing apoptosis of cardiac myocytes within 24 h after MI, suggesting that TNF-α may protect cardiac myocytes from ischemic injury by preventing apoptosis. Furthermore, pre-MI treatment with TNF-α has been shown to ameliorate ischemic/reperfusion injury with induction of MnSOD [23]. These results suggest that the pathophysiological roles of TNF-α in the subacute phase of MI (more than 3 days) may be different from those in acute ischemia (within 24 h). TNF-α may protect cardiac myocytes from cell death in acute ischemia, but promote apoptosis of infiltrating cells to resolve inflammation in the subacute phase.

Myocardial infarction leads to complex structural alterations in both infarct and non-infarct myocardium, resulting in progressive dilatation and dysfunction of the ventricle (remodeling). TNF-α is induced in the failing human heart [2]. Its role in the progression of ventricular remodeling is inferred from findings that TNF-α suppresses cardiac contractility [3], provokes myocardial hypertrophy [4], and induces apoptosis in cultured cardiac myocytes [5]. However, in the present study, treatment with soluble TNFR1 further exacerbated ventricular dysfunction and remodeling even when given after the acute phase. These results suggest that TNF-α may protect infarct and non-infarct myocardium from the progression of remodeling. The dynamics of synthesis and breakdown of ECM proteins play an important role in post-MI LV remodeling. In particular, increased expression and activation of MMPs have been implicated in this process [21]. Several studies have demonstrated that MMPs are involved not only in cardiac rupture [19,22] but also in LV remodeling and failure [24,25]. Among the known MMPs, MMP-2 and MMP-9 have been shown to play an important role in post-MI remodeling [19,24]. Although MMP-9 is

mainly expressed in infiltrating inflammatory cells such as neutrophils and macrophages, MMP-2 is ubiquitously distributed in cardiac myocytes and fibroblasts and is up-regulated after MI. In the present study, we have demonstrated that post-MI treatment with soluble TNFR1 further activates MMP-2 in non-infarct myocardium, while the pre-MI treatment augments MMP-9 in infarct myocardium. Furthermore, we have previously reported that targeted disruption of MMP-2 as well as MMP-9 attenuates not only ventricular rupture but also ventricular remodeling after MI [19]. Therefore, exacerbation of ventricular remodeling and dysfunction after TNFR1 treatment may be mediated by further activation of MMP-2, although the precise mechanism by which MMP-2 is further activated remains undetermined.

The present findings contradict the results of Sun et al. [12] using TNF-α knockout mice. Targeted disruption of TNF-α by gene knockout significantly reduced acute cardiac rupture and improved chronic left ventricular dysfunction after MI, accompanied by a reduction of cardiac inflammatory cell infiltration, cytokine expression, and MMP-9 activity. Chronically, TNF-α knockout mice also showed less fibrosis and apoptosis in the myocardium remote from the infarct zone, which contributed to improved ventricular function [12]. These results are thoroughly opposite to ours. Although gene targeting completely eliminated TNF-α in myocardium, the absence of TNF-α during embryogenesis and development may have altered other signaling pathways to secure physiological growth of these mice. Therefore, the differences between the present study and the previous report may be attributed to the methods adopted to block the effects of TNF-α.

TNF-α initiates its biological effects by binding two distinct cell surface receptors with approximate molecular masses of 55 kDa (TNFR1) and 75 kDa (TNFR2) [1]. Both receptors are expressed in most cell types, including cardiac myocytes. Although most biological activities of TNF-α are signaled through TNFR1, the role of TNFR2 remains unclear. Targeted disruption of TNFR1 has been shown to reduce ventricular rupture and remodeling after MI [13]. Furthermore Higuchi et al. [26] have recently demonstrated that ablation of TNFR1 ameliorated heart failure and improved survival while ablation of the TNFR2 gene exacerbated heart failure and reduced survival of TNF-α transgenic mice, suggesting a cardioprotective role of TNFR2-mediated signaling. Therefore, exacerbation of ventricular rupture and remodeling observed in the present study may have derived from blockade of TNFR2-mediated signaling. Because the dissociation constants of TNFR1 and TNFR2 are $2–5 \times 10^{-10}$ and $3–7 \times 10^{-11}$, respectively [1], high levels of TNF-α interact with both TNFR1 and TNFR2, while low levels may only stimulate TNFR2 pathways. In other words, low levels of soluble TNF receptors may only block cytotoxic TNFR1, whereas high levels of soluble TNF receptors may also block the protective TNFR2. Because plasma levels of soluble TNF receptors in the present study (about 500 μg/ml) were more than 100 times higher than clinical plasma levels (approximately 0.3–3 μg/ml) [27], these high levels may block the protective TNFR2 resulting in deleterious results. Using lower doses of soluble TNF receptors may produce different results.

Another explanation for the negative results of the present study might be intrinsic toxicity of soluble TNF receptors [7]. Soluble TNF receptor also acts as a carrier protein that stabilizes TNF-α resulting in the accumulation of high concentrations of immunoreactive TNF-α [18]. Because binding of TNF-α–TNFR complexes is reversible [28], the increase in level of TNF-α–TNFR complex may lead to an increase in the duration of TNF bioactivity. Specifically, this might be the case for soluble TNFR2 fusion proteins, including etanercept that was used in RENEWAL [8]. Studies of the binding of TNF-α with soluble TNF receptor fusion proteins have shown that TNFR2 exchanges bound TNF-α about 50- to 100-fold faster than TNFR1 [29]. Thus, although both fusion proteins in equilibrium bind TNF-α with high affinity, the TNF-α–TNFR1 fusion protein complex is kinetically more stable than the TNFR2 fusion construct. Because the soluble TNF receptors used in the present study were TNFR1, the intrinsic toxicity might have been less than that if TNFR2 were used. To confirm this hypothesis, we measured the bioactivity of TNF-α in the myocardium, and found that the bioactivity was significantly reduced by the treatment. Therefore, this might not be the case in the present study.

Although the negative results of anti-TNF clinical trials in patients with heart failure prompted us to conduct the present study, there are several important aspects that are different between the present study and the clinical trials. First, acute myocardial infarction was used as a model of heart failure in the present study, while patients with chronic heart failure were recruited in the clinical trials. The roles of proinflammatory cytokines might be different in acute and chronic phases of myocardial infarction. Second, the dosage of soluble TNF receptors used in the present study was more than 100 times higher than that used in the clinical trials. Effects of high doses should be different from those of lower doses, which remain undetermined in this mouse MI model. Therefore, caution has to be exercised in interpreting the present results in association with the clinical trials.

In conclusion, treatment with soluble TNF receptors increases ventricular rupture and exacerbates cardiac remodeling in a murine model of MI. Because TNF-α seems to play both cytotoxic and protective roles in cardiovascular diseases, further studies are required to elucidate the optimal approach to modulate proinflammatory cytokines in clinical practice.

Acknowledgments

A part of this study was conducted in Kyushu University Station for Collaborative Research. This study was supported by a grant from Kimura Memorial Heart Foundation, by the Grant for Research on Cardiovascular Disease from Japan Heart Foundation/Pfizer Pharmaceuticals Inc., by the Grant-in-Aid for Scientific Research from the Japan Society for the promotion of Science (C15590755), by the Health and